QUANTUM CARBON DOT-GOLD NANOPARTICLE HYBRID NANOMATERIALS AS NEW GENERATION CONTRAST AGENTS IN BIOIMAGING

by

Buğra Onat

Submitted to Graduate School of Natural and Applied Sciences
in Partial Fulfillment of the Requirements
for the Degree of Master of Science in
Biotechnology

Yeditepe University
2023

QUANTUM CARBON DOT-GOLD NANOPARTICLE HYBRID NANOMATERIALS AS NEW GENERATION CONTRAST AGENTS IN BIOIMAGING

APPROVED BY:

Prof. Dr. Fikrettin Şahin ……
(Thesis Supervisor)
(Yeditepe University)

Prof. Dr. Gamze Torun Köse ……
(Yeditepe University)

Prof. Dr. Deniz Ceylan Tuncaboylu ……
(Bezmialem University)

DATE OF APPROVAL: ..../..../2023

I hereby declare that this thesis is my own work and that all information in this thesis has been obtained and presented in accordance with academic rules and ethical conduct. I have fully cited and referenced all material and results as required by these rules and conduct, and this thesis study does not contain any plagiarism. If any material used in the thesis requires copyright, the necessary permissions have been obtained. No material from this thesis has been used for the award of another degree.

I accept all kinds of legal liability that may arise in case contrary to these situations.

Name, Last name Buğra Onat

Signature …..…….……..

ACKNOWLEDGEMENTS

I am very grateful to Prof. Dr. Fikrettin Şahin, who has constantly guided me in my graduate life and supported me with his knowledge and academic environment.

Since the day we met, they have put up with someone like me, who has not lacked in joy and fun, and who has no understanding of chemistry and materials science, for such a long time. who has always guided me and made me improve myself so much. I would like to express my endless thanks to Dr. Zeliha Cansu Canbek Özdil and Dr Volkan Can.

For always supporting me whenever I have a problem since the day I was born, never giving up on me, and constantly helping me despite all the troubles I went through during this graduate program. I would like to express my endless gratitude to my mother, Gülşen Binbay, who gave me all kinds of financial and moral support and whom I loved more than anything, even though I did not have any financial strength while embarking on this journey.

Lastly, my destiny partners, I would like to thank İlayda Set and Hazar Soydan, and Turkucan Erdem who we always helped each other when we were in trouble, we got through a difficult 3 years together, we laughed and cried.

ABSTRACT

QUANTUM CARBON DOT-GOLD NANOPARTICLE HYBRID NANOMATERIALS AS NEW GENERATION CONTRAST AGENTS IN BIOIMAGING

Carbon dot-gold nanoparticle hybrid systems [CD/AuNP) show great potential for biological imaging of cancer due to the enhanced photoluminescence capability arising from the synergistic coupling between the carbon dots and the gold nanoparticles called fluorescence resonance energy transfer (FRET). Compared to conventional dyes, CD/AuNP hybrid systems do not exhibit bleaching effects, so their fluorescence capacity does not decrease over time. Also, this hybrid system does not exhibit cellular cytotoxicity. Traditionally, CD/AuNP hybrids are prepared separately by wet chemical methods and then mixed together. Namely, both nanoparticle solutions (CD and AuNP) are prepared in different reaction containers and then mixed together to obtain the hybrid. However, in the proposed solid-state synthesis method, it is possible to prepare the hybrid in the same reaction container, which shortens the time and increases the photoluminescence yield of the nanoparticles. The aim of this study is to investigate the photoluminescence properties of CD/AuNP hybrid systems obtained with different reaction parameters via a one-pot solid-state synthesis method. The photoluminescent properties of the synthesized particles were investigated by using fluorescent spectroscopy. The particles were used as cellular imaging agents on different cancer cell lines such as A549, Panc02, and MCF -7. HDF was used as a control. Afterward, the cellular proliferation capacity, cellular cytotoxicity, and bio-imaging properties of the CD /AuNP systems were analyzed to find the most effective system for further studies.

ÖZET

BIO GÖRÜNTÜLEMEDE YENİ NESİL KONTRAST AJANLARI: KUANTUM KARBON NOKTA-ALTIN NANOPARTİKÜL HİBRİT NANOMALZEMELER

Karbon nokta-altın nanoparçacık hibrit sistemleri (CD/AuNP), karbon noktalar ve altın nanoparçacıklar arasındaki floresan rezonans enerji transferi (FRET) adı verilen sinerjik bağlantıdan kaynaklanan gelişmiş fotolüminesans kabiliyeti nedeniyle kanserin biyolojik görüntülenmesi için büyük potansiyel göstermektedir. Geleneksel floroforlu görüntüleme ajanları ile karşılaştırıldığında, CD/AuNP hibrit sistemlerinde floresans yoğunluğunda zamanla azalma görülmemiştir. Ayrıca, CD/AuNP hibrit sistemleri hücresel sitotoksisite göstermemektedir. Genel olarak, CD/AuNP hibrit malzemeler ıslak kimyasal yöntemlerle ayrı ayrı hazırlanır ve daha sonra karıştırılır. Yani, her iki nanoparçacık çözeltisi (CD ve AuNP) farklı reaksiyon kaplarında hazırlanır ve daha sonra hibriti elde etmek için karıştırılır. Ancak katı hal sentez yönteminde hibriti aynı reaksiyon kabında hazırlamak mümkündür. Bu çalışmanın amacı, tek-pot katı hal sentez yöntemi ile farklı reaksiyon parametreleri ile elde edilen CD/AuNP hibrit sistemlerinin fotolüminesans özelliklerini incelemektir. Sentezlenen partiküllerin fotolüminesans özellikleri floresan spektroskopisi kullanılarak araştırılmıştır. Partiküller, A549, Panc02 ve MCF -7 gibi farklı kanser hücre hatları üzerinde hücresel görüntüleme ajanları olarak kullanılmıştır. Daha sonra, CD /AuNP sistemlerinin hücresel çoğalma kapasitesi, hücresel sitotoksisite ve biyo-görüntüleme özellikleri, analiz edilmiştir.

TABLE OF CONTENTS

LIST OF FIGURES

LIST OF TABLES

LIST OF ABBREVIATIONS/ SYMBOLS

AuNP	Gold nanoparticule
AuNR	Gold nanorod
CD	Carbon dot
DLS	Dynamic light scattering
MEF	Metal enhanced fluorescence
PI	Propidium iodide
QL	Quantum confinement effect
SPR	Surface Plasmon Resonance
SSNP	Solid state nanoparticule
UV-Vis	Ultraviolet-visible

1. INTRODUCTION

1.1 CARBON-QUANTUM DOTS

1.1.1 Properties and Aplications

Organic fluorescent dyes are commonly used in biological imaging applications such as biomolecular labeling, cancer diagnosis, etc. Their emission profile can be varied depending on the type of fluorophore group in their chemical structure and in general, they are within the size range of 2-10 nm [1-3]. However, these organic dyes have limitations such as poor fluorescence stability, weak photobleaching resistance, and short fluorescence lifetime, which restrict their practical use. They can also cause toxicity at high concentrations. Additionally, they have low temporal stability, meaning that they can evolve within time, and have low water solubility, so they require an organic solvent during preparation [4].

Nanomaterials are a class of materials having at least one dimension below 100 nm [5]. With the recent progress in nanotechnology in the last decade, the development of new-generation biocompatible nanomaterials bearing photoluminescent properties as an alternative to organic dyes is gaining high importance to overcome the previously listed challenges [6-8]. Emerging nano fluorescent materials like semiconductor quantum dots (QDs) and carbon dots (CDs) are becoming more popular due to their excellent physical and chemical properties. These materials are not only used for biological imaging and targeting tumor cells, but also find applications in drug and gene delivery, biosensors, medical treatment, photocatalysis, electrocatalysis, and more [9].

Semiconductor QDs have sizes below 10 nm and possess a size-dependent emission spectrum with a fluorescence lifetime typically ranging from a hundred to a few hundred nanoseconds. However, they have poor stability under UV light and can contain heavy metals in their structure, which means that degradation of the material could cause potential toxicity in biological systems [10].

In contrast, CDs, are typically made from carbon-rich sources such as carbon nanotubes, graphene, or carbon-containing precursors such as citric acid, making them inherently less likely to be toxic [11].

They show emission in the UV-Vis and near-infrared (NIR) regions and the lifetime of CD is similar to that of organic dyes. Moreover, they can easily be dissolved in water. The surface of CDs can be functionalized with various surface groups, such as hydroxyl (-OH) or carboxyl (-COOH) groups, which can enhance their biocompatibility. These functional groups can help reduce the toxicity of CQDs by improving their solubility, and stability, and reducing potential interactions with cellular components [12,13].

1.1.2 Synhtesis of Carbon Dots

Usually, CDs are prepared by hydrothermal synthesis methods using multiple carbon precursors. Citric acid, urea, polyethylene glycol (PEG), sodium tri-citrate dihydrate, ascorbic acid, and glucose are some of the commonly used precursors [14]. Depending on the carbon source and reaction conditions, it is possible to tune the optical properties of the material. For instance, aliphatic carbon sources such as citric acid often exhibit blue or green fluorescence emission, with emission peaks typically ranging from 400 to 500 nm whereas, carbon dots synthesized from PEG typically exhibit red or near-infrared (NIR) fluorescence emission, with emission peaks ranging from 600 to 800 nm. However, when the carbon source is replaced by aromatic compounds, the color of the resultant material changes to yellow. In the charring process, functional groups on the surface of the molecule that has been reduced by the luminescent groups on the surface have a direct effect on the charring process [15,16].

It is also possible to obtain highly fluorescent blue-emitting CDs via a carbonization reaction between citric acid and Ethylenediamine (EDA) at high temperatures via hydrothermal autoclave synthesis [17].

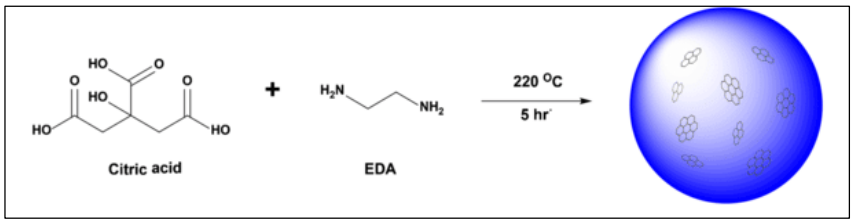

Figure 1.1 Schematic illustration of the synthesis of CDs by citric acid and EDA

1.2 GOLD NANOPARTICLES

Metallic nanoparticles have gained significant attention in the biomedical field due to their unique properties such as ease of production, easy surface functionalization, and versatility, which make them suitable for various applications [18]. They exhibit unique optical and magnetic properties that can be harnessed for various biomedical applications.

Especially, gold nanoparticles are extensively being studied for imaging, photothermal therapy, and diagnostics due to their exceptional optical properties. Namely, when gold nanoparticles are excited by photons of the incident light, the conduction electrons of the gold nanoparticle absorb the energy from the incident light and start to oscillate collectively at a certain frequency which is known as the surface plasmon resonance (SPR) frequency [19]. The SPR in gold nanoparticles leads to a distinctive absorption spectrum, which is highly dependent on the size, shape, and surrounding environment of the nanoparticles [20]. By carefully controlling the size, shape, and surface chemistry of gold nanoparticles, their SPR can be fine-tuned to achieve desired optical properties for various applications, such as in sensing, imaging, and photothermal therapy. SPR in gold nanoparticles has been widely exploited for biosensing applications, where changes in the local refractive index near the surface of the nanoparticles, caused by biomolecular interactions, can be detected as shifts in the SPR wavelength. This has led to the development of gold nanoparticle-based SPR biosensors that offer high sensitivity and specificity for detecting various biological analytes, such as proteins, nucleic acids, and small molecules [21]. Gold nanoparticles can be readily prepared by thermal reduction HAuCl4 in the presence of sodium tri-citrate. The size of the nanoparticles can be tuned by optimizing the concentration of sodium tri-citrate in the reaction. Citrate is used as a capping agent to prevent the aggregation of the nanoparticles [22].

1.3 CARBON DOT-GOLD NANOPARTICLE HYBRIDS

Hybrid nanomaterials provide different properties in the field of imaging. Combining two different components becomes one and unique components. CD and AuNP have different unique properties, and while they come together, they also share these unique properties in the same structure [23].

Two main effects are important for the carbon-dot gold nanoparticle interaction. The first of these is that the carbon dots have a unique electrochemical property, such as the quantum confinement effect. Quantum confinement effects (QCE) occur in nanoparticles in the 2-10nm range and determine the PL emission wavelength due to its size [24]. The second effect is metal-assisted fluorescence (MEF), because when electrons in CD are excited by light excitation, these excited electrons interact with the surface electrons of the gold nanoparticle. This interaction increases the fluorescence capacity of CD [25].

In 2014, Shi et all combines gold nanoparticles with carbon dots using the wet chemistry method. During their synthesis, citric acid and 2,2,'-(ethylene-deoxy) bis(ethylamine) were used for carbon points and HAuCl4 3 H2O for gold and microwave was used to initiate the reactions. With this they produced pH sensitive CD for intracellular imaging [26] In 2018 Pal et all shows that combining different stabilization methods applied CD and AuNPs together shows a MEF effect on CD. They show that the PL capacity of CD can be enhanced by a combination of AuNPs [27]

1.4 CARBON DOT-BASED MATERIALS IN CANCER IMAGING AND DIAGNOSIS

Cancer is a disease in which healthy cells lose control of their growth and begin to grow immeasurably. This uncontrolled cell division then begins to attack other cells in the body. A cancer diagnosis is becoming more important every year because early diagnosis increases the efficiency of treatment [28]. Every year, millions of people are diagnosed and suffer from cancer. Various factors in the body can contribute to the development of cancer, but there are some key characteristics that can be used to distinguish cancer cells. Firstly, cancer cells have the ability to continuously increase growth signals, while also reducing the effects of growth suppressors by increasing the activity of EGFR initiators and cyclin-dependent

kinase inhibitors, allowing them to bypass growth suppressors [29]. Additionally, cancer cells can increase the production of pro-apoptotic proteins like BH3 mimetics, which help them avoid cell death [30]. Cancer cells can also evade the immune system by concealing themselves from immune cells and activating anti-CTLA-4, leading to tumor progression in the cancer microenvironment [31]. Furthermore, cancer cells can become immortal by inhibiting telomerase activation through the use of PARP inhibitors, as the genome of cancer cells is inherently unstable, leading to uncontrollable mutations [32]. Moreover, cancer cells can create their own venous system, known as angiogenesis, and then spread to other organs, a process called metastasis [31,33].

In the early detection of cancer, imaging is a powerful tool. Yet, cancer imaging encounters challenges due to the presence of receptors not only in cancer cells but also in healthy cells. For instance, the folate receptor is found in both hematomas and breast cells, which makes it difficult to achieve selectivity in imaging. However, researchers have improved selectivity in imaging studies by utilizing folic acid-conjugated CDs, which are a type of imaging agent [34].

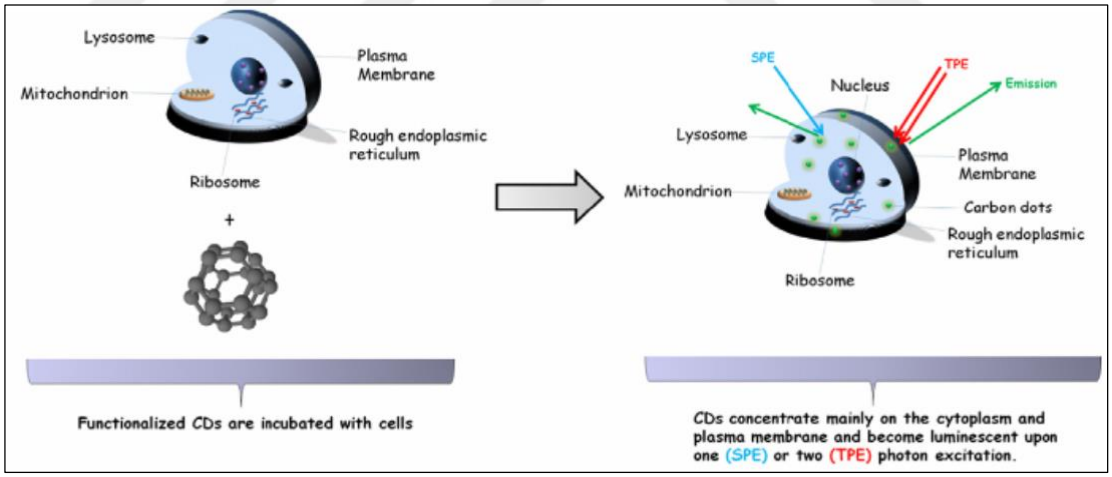

Figure 1.2 Representative image of CDs bioimaging [35]

In the (Figure 1.2) shows the necessary steps in the visualization of cells in confocal microscopy by using CDs as a labeling agent. CDs were absorbed into the cell by diffusion. Then the nanoparticle accumulates in the cytoplasm. When the cells are excited with the incident light, CDs, which are in the endosomal region, exhibit fluorescence emission which is used for confocal microscopy imaging [35].

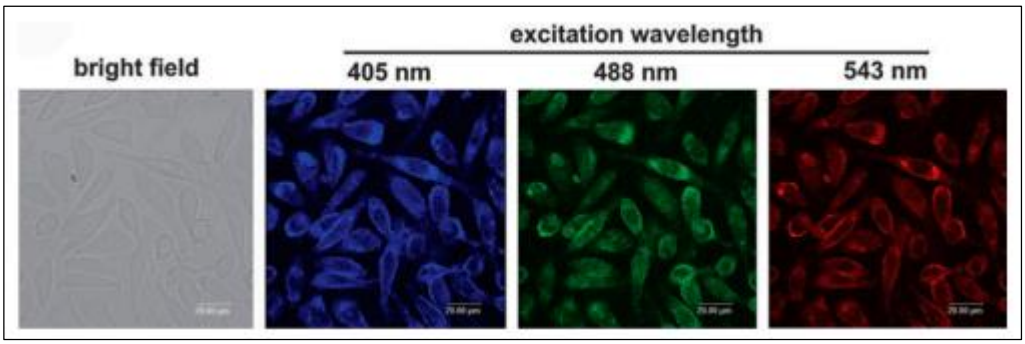

Figure 1.3 Representative image of Nitrogen-doped carbon dots confocal images with 488 nm excitations 540 nm emission. With DAPI nuclei staining [37]

In 2021, Zhai and his team demonstrated that their CDs are capable of emitting different fluorescent lights at different excitation wavelengths as shown in (Figure 1.3) [36]. In this work, the L-929 cells were treated with the CDs and then excited at three different wavelengths (405, 488, and 543 nm) yielding blue, green, and red emissions.

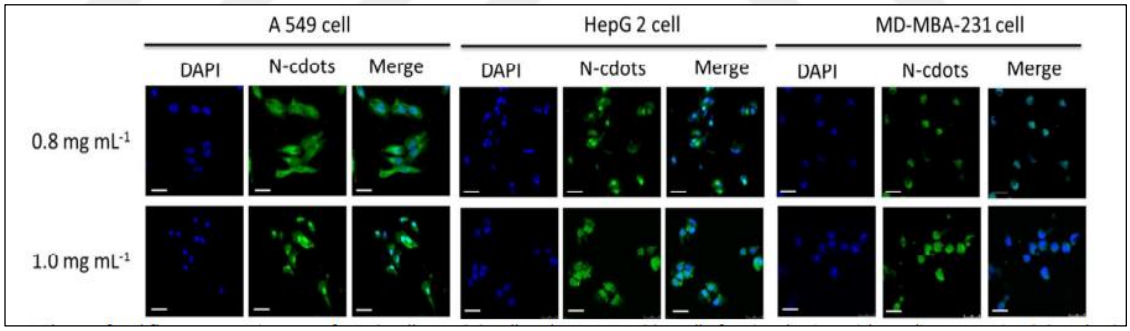

Figure 1.4 Representative image of Nitrogen-doped carbon dots confocal images with 488 nm excitations 540 nm emission. With DAPI nuclei staining [37]

In 2015, Kang and his team showed that nitrogen-doped carbon dots, synthesized by using dopamine as a precursor, can be used to visualize and investigate the function of the nuclear membrane [37]. In this work, different cell lines were incubated with nitrogen-doped CDs at different concentrations and compared with DAPI which is used as a control (Figure 1.4). It is indicated that small size, positive surface charge, and the presence of dopamine-mimicking functional groups are critical parameters for entrance into the nuclear membrane.

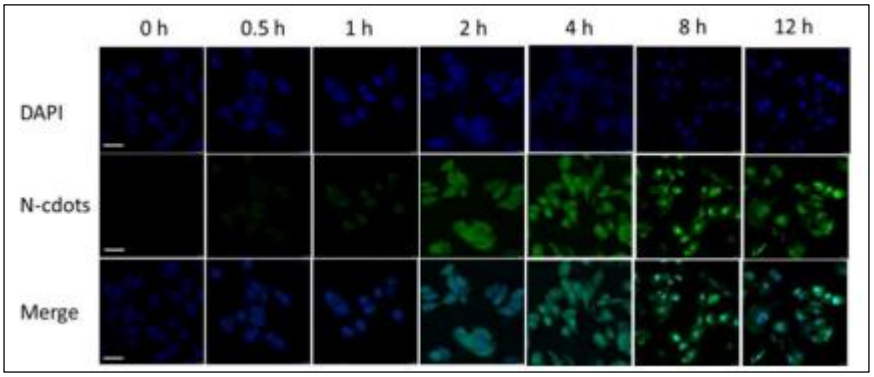

Figure 1.5 Confocal image of CD treated A549 with different time periods.[37]

In 2007, Li Cao and his colleagues reported that CDs are visible inside the cell membrane but cannot diffuse into the cell nuclei [38]. This is because CDs can bind with DNA and RNA in the cell membrane due to their strong positive charge. In 2014, Datta succeeded in bringing CDs into cell nuclei by combining cationic quaternized CD with anionic graphene oxide films [39]. In their research, they show that their hybrid nanomaterials act like probes and localize in the nuclei of NIH/3T3 cells [39].

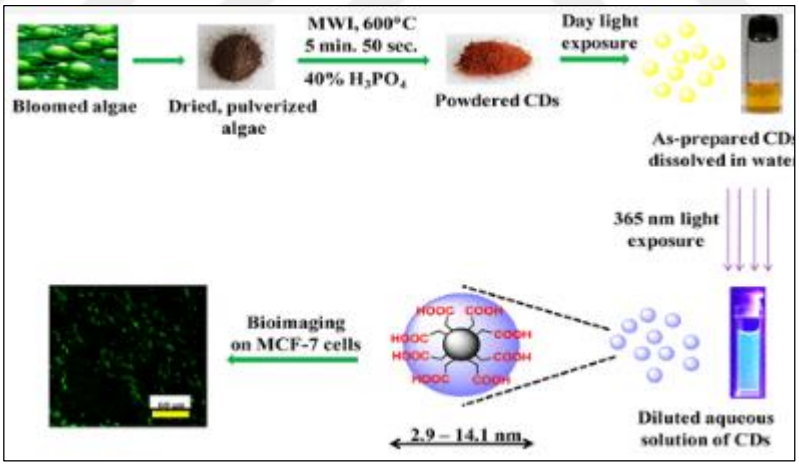

Figure 1.6 Representative image of green synthesis of CDs [40]

Ramanan and his co-worker [40] show that CDs can also be synthesized by using biological compounds such as Biomed algae as a carbon source (Figure 1.6). With natural carbon sources, the CDs show excellent cell permeability with high photostability. When they treated their CDs with MCF -7 cell lines, they also reported that CDs can be used as potential biomarkers [40].

Furthermore, multiple studies have demonstrated that carbon dots (CDs) are not only limited to in-vitro applications but can also be used effectively in in-vivo applications. (Figure1.7) illustrates that when CDs are injected into mice in vivo near-infrared (NIR) fluorescence imaging can be realized. The efficiency of excitation and emission may vary depending on the CDs properties. In 2018, it was reported that fluorescently labeled CDs were utilized for cancer diagnosis [41]. These systems have also been found to have potential in cancer theranostics, as CD-based silica nanostructures can cross the blood-brain barrier due to their ultra-small particle size [41].

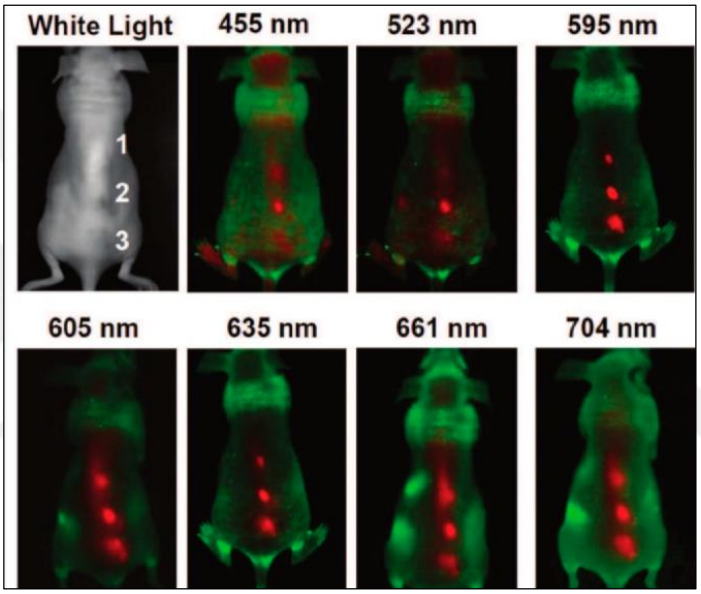

Figure 1.7 In-vivo application of the CD. Different Execution emission application result image of the CD in in-vivo [42]

1.4.1 Carbon Dot/Gold Nanoparticles

CD/AuNP hybrids systems can be a sensing material to detect glucose levels [117]. Also, hormone quantification can be made by using this hybrid system by taking advantage of the inner filter effect. The inner filter effect (IFE) of AuNP on the fluorescence of graphene quantum dots serves as the foundation for the fluorescent dopamine assay. In the presence of citrate-stabilized AuNPs, IFE significantly inhibits the green fluorescence of GQDs. Dopamine causes the AuNPs to aggregate, which is indicated by a switch in color from red to blue. GQDs' fluorescence is restored and the IFE is no longer possible [43].

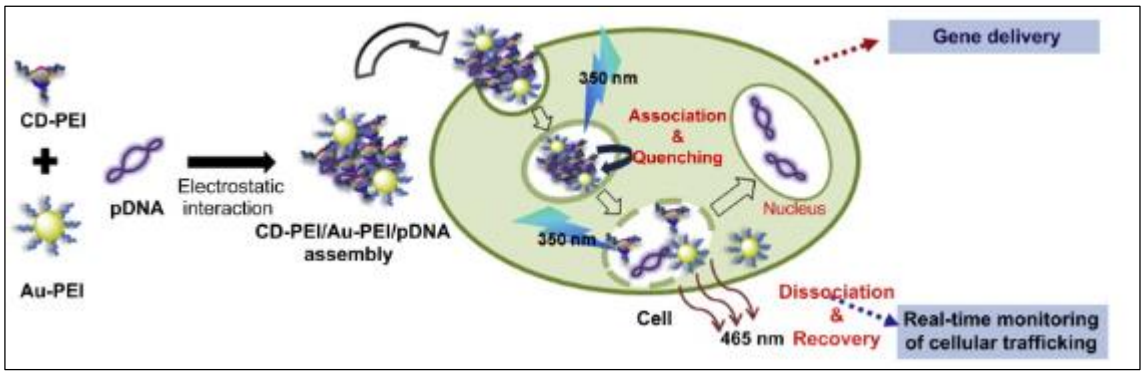

Figure 1.8 CD-PEI and AU-PEI used a hybrid particular system with the attachment of Pdna s used for gene localized gene delivery and bio-imaging together [44]

Also, CD/AuNP derivatives (GNR@SiO2@CDs which are gold nanorods and CDs bridged with silica) can be used for the detection of atherosclerosis by using fluorescence lifetime imaging microscopy (FLIM) measurements (Figure 1.9). In this study, it is demonstrated that it is possible to identify the accumulation of macrophages by using hybrid nanoparticles based on carbon dots, which is a well-known indicator of unstable atherosclerotic plaques [45].

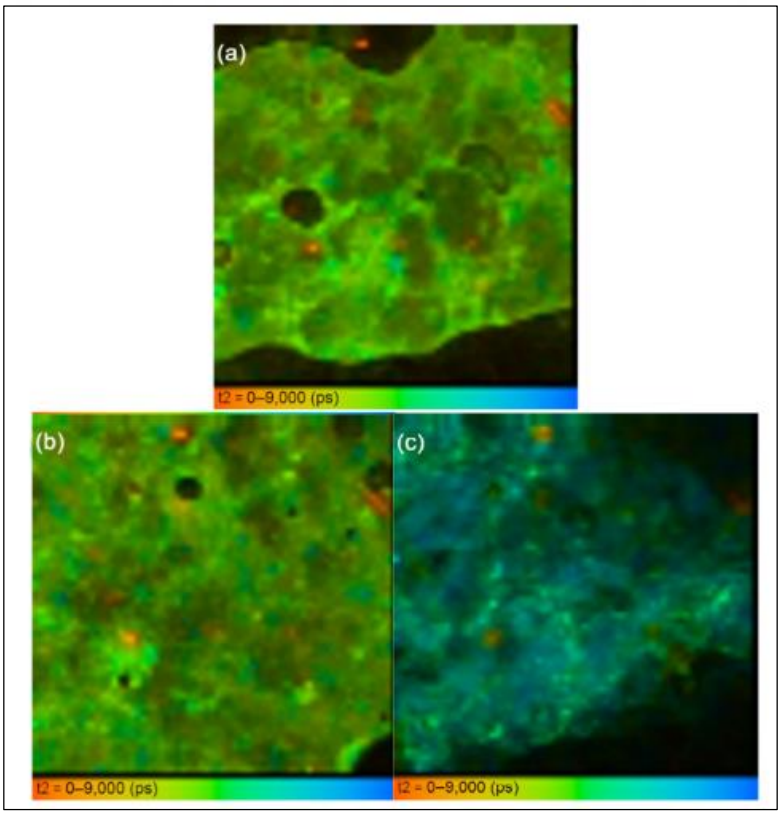

Figure 1.9 Fluorescence lifetime microscopy images of phantoms prepared by using (a) macrophages (b) macrophage+CD and (c)macrophages+GNR@SiO2@CDs [45]

2. MATERIALS

Tetra chloroauric (III) acid trihydrate ($HAuCl_4.3H_2O$), citric acid (CA), sodium tri-citrate dihydrate, and ethylene diamine (EDA) were obtained from Sigma Aldrich and used without further purification. Prior to experiments, all glassware was cleaned with aqua regia and washed with distilled water.

Dulbecco's Modified Eagle Medium (DMEM) with High Glucose (4.5g/L), L-glutamine-Phenol Red without sodium pyruvate and HEPES (GIBCO Catalog Number: 11965092) - Roswell Park Memorial Institute (RPMI) 1640 medium with L-glutamine, phenol red and sodium bicarbonate buffer system without HEPES. (GIBCO catalog Number 11875093) - Trypsin/EDTA cellular dissociation reagent contains 0.025%trypsin and 0.01%EDTA with phenol red. (Catalogue number R001100) – Penicillin-Streptomycin-Neomycin (PSN) solution contains 5 mg of penicillin, 5mg of streptomycin, and 10mg of neomycin in 1 ml in 0.85% saline solution (GIBCO catalog number 1564055). 1X Dulbecco's phosphate-buffered saline (DPBS) without phenol red, calcium, and magnesium (GIBCO catalog number 14190144). Heat Inactivated Fetal Bovine Serum (FBS) (GIBCO Cat number10082147). Dimethyl Sulfoxide (DMSO) ≥ 99.9% (Merck Cas Number 67-68-5). D-glucose (dextrose) Powder (GIBCO Catalogue no 15023021). eBioscience™ Annexin V Apoptosis Detection Kit (Invitrogen Catalogue number BMS500FI-300). BioVision MTS reagent (Cat no 2808), Glentham Life Sciences Hydrogen tetrachloroaurate(III) trihydrate (Cas No 16961-25-4), Sigma-Aldrich Citric Acid (Cat no 251275-100G), Merck ethylenediamine (Cas no 107-15-3), Merck Absolute methanol (Cat No 1037261002).

T75 TPP tissue culture flask (Cat no Z707546), 6 Well Plate TPP tissue culture flask (Cat no Z707767-72EA), Corning 96 well plate TC-Treated microplate (Cat no CLS3997), Corning Falcon 15 ml Conical Centrifuge Tubes (Cat no 14-959-53A), Corning Falcon 50 ml Conical Centrifuge Tubes (Cat no 14-432-22), ISOLAB Colour End Microscope Slide (Cat no 075.02.005), ISOLAB 20x20MM coverslip (Cat no 075.00.002). Cambridge Energy Solutions Hydrothermal Synthesis Autoclave Reactor with PTFE Lined Vessel 50ml (SS-AC-50).

Human Epithelial Lung Adenocarcinoma (A549), Primary Adult Human Dermal Fibroblast (HDF), Epithelial Breast Adenocarcinoma (MCF-7), and Pancreatic epithelial adenocarcinoma (Panc 02.03) were purchased from American Type of Cell Collection.

3. METHODS

3.1 SYNTHESİS OF CQD/AuNP HYBRID

Table 1 represents the chemical compositions of the samples. All components were dissolved in distilled water after the synthesis. All of the reagents in Table 1 were prepared separately in same-sized and same-brand beakers. During the synthesis, the first citric acid was weighed and mixed with water. Then the EDA was added to the solution inside the fume hood. The sample is stirred with a magnetic stirrer for 10 minutes. Afterward, a defined amount of HAuCl4 was added under magnetic stirring and the resultant solution was dried in the oven at 65°C overnight. Following, the temperature is set to 160°C and the sample was placed in the incubator for 2 hours. In the end, the sample was taken out and left for 1 hour at room temperature. Then the samples were dissolved in 10 ml of distilled water. The characterization was realized on the following day of the synthesis.

Table 3.1. Sample information and the amount of reactants ısed during the synthesis

Sample No	Citric Acid (g)	EDA (g)	0.1 M $HAuCl_4$ (ul)
SS1	0.9602	0.15	0
SS2	0.9602	0.3	0
SS3	0.4830	0.3	0
SS4	0.9602	0.15	25
SS5	0.9602	0.3	25
SS6	0.4830	0.3	25
SS7	0.9602	0.15	50
SS8	0.9602	0.3	50
SS9	0.4830	0.3	50
SS10	0.9602	0.15	100
SS11	0.9602	0.3	100
SS12	0.4830	0.3	100

3.2 CHARACTERIZATION OF CQD/AuNP HYBRID

3.2.1 UV-Vis Spectroscopy

The spectra of the synthesized particle were analyzed by using PerkinElmer LAMBDA 25 series UV-Vis Spectrometer. After the reactions, all of the reagents and distilled water were taken. 3ml of distilled water was put in cuvettes as a blank and 3ml of all the reagents in a dilution of 1:500 with distilled water also were put in another cuvette. Spectroscopy device were set for (240lambda for one minute). Before the reading of each sample, every time device settings were set for auto-zero. After the reading of each sample absorbance versus nm plots were drawn.

3.2.2 Fluorescence Spectroscopy

Fluorescence measurements were carried out using HORIBA DUETTA Absorption and Fluorescence Spectrometer. After the reactions, all of the reagents and distilled water were taken. 3ml of DI water was put in cuvettes as a blank and 3ml of all the reagents in a dilution of 1:500 with distilled water also were put in another cuvette. Spectroscopy devices were set for (300lambda to 675lambda). Before the reading of each sample, every time device settings were set for auto-zero. After the reading of each sample intensity/emission wavelength plots were drawn.

3.2.3 Dynamic Light Scattering (DLS)

Dynamic Light Scattering and Zeta Potential analysis were made with MALVERN Instruments. All of the measurements were made at a room temperature of 25 °C. Each measurement was repeated three times to increase the quality of the measurement.

3.2.4 Transmission Electron Microscopy

TEM observations were carried out by using JEOL JEM 2100 Plus microscope attached to Gatan US4000 CCCD camera. 10ul of all of the samples were dropped into TEM grids.

Samples were put in room temperature for 24h to samples were dry. TEM images were taken respectively.

3.3 CYTOTOXICITY AND BIOIMAGING EXPERIMENTS

3.3.1 Cell Culture Conditions

HDF, MCF-7, and A549 cells proliferated in DMEM medium which is conditioned with 10% FBS and 1%PSA respectively. Panc 02.03 cells were grown in RPMI 1640 medium which is conditioned with 10% FBS and %1 PSA respectively. Cells were cultured in an ESCO Class II A2 biosafety cabinet which is continuously giving normal conditions such as 37°C %5 CO_2 and %80 air humidity.

3.3.2 Cell Passaging

PANC-1, PANC 02.03, and HPNE cells were treated with 100 μM ST and placed into air-jacketed CO_2 incubator conditioned to 37°C with 5% CO_2 for 24 H incubation. For Annexin V+PI, treatment was performed also for 48 H, and for MTS treatment time was performed for 24, 48, and 72 H.

3.3.3 MTS Cellular Proliferation Assay

After the passaging of each cell line cells were taken and seeded into a new 96-well plate in a concentration of 5000 cells/well in 100ul fresh cell culture medium. After that cells were put into a hood overnight for cellular attachment. After that, all of the old culture mediums were discarded. Then cells were treated with different concentration dosage of CQD/AuNP nanohybrid particles which is given in the table. After that cells were incubated in the hood for 24-48-72h respectively. After each time point has come. The old cell culture medium was discarded and cells were washed with 100ul 1X PBS. After that tetrazolium salt was mixed with (4.5 grams/liter) glucose containing 1X PBS in a ratio of 1:10. After that cells were treated with 100 ul MTS mixture for 2h. Then UV-Vis Absorption spectroscopy results in 490nm of each well were taken using ELISA Plate Reader by BioTek Instruments.

3.2.4 Annexin-V Apoptotic Cell Assay

All of the flow cytometry measurements were made by using the Millipore Corporation guava easyCyteTM flow cytometer device. After the passaging of each cell line cells were taken and seeded into a new 6-well plate in a concentration of 300.000 cells / well in a 1ml fresh cell culture medium. After that cells were put into a hood overnight for cellular attachment. After that, all of the old culture mediums were discarded. Then cells were treated with different concentration dosage of CQD/AuNP nanohybrid particles which is given in the table. After that cells were incubated in a hood for 24 respectively. After that cells were taken with the usage of Trypsin EDTA. After that, all of the cells were washed with 1X PBS. After each wash cells were centrifuged for 1500rpm for 5 minutes at room conditions. After that cells were suspended with 1X binding buffer which is containing 5ul of annexin-v-FITC antibody. Cells were incubated at 20 minutes room temperature at dark. After that cells were washed twice with 1X binding buffer. Then before the flow cytometry reading 3ul of PI was added to each sample.

3.2.5 Confocal Microscopy Assay

Microscope cover slides were taken in the bio-safety 2 cabinets. And before the using all of the cabinet were UV sterilized for 1h. After that Microscope slides washed with %70 EtOH than they were put into the 6-well plate. After that all of the well plate were UV sterilized in a biosafety cabinet. After that cell lines were passaged then every 200.000 cells were seeded on the cover slide containing the microscopy slide. After that cells were put into a hood overnight for cellular attachment. After that, all of the old culture mediums were discarded. Then cells were treated with different concentration dosage of CQD/AuNP nanohybrid particles which is given in the table. After that cells were incubated in a hood for 24h respectively. Then all of the wells containing cells were washed with 1ml of 1X PBS twice. Then ice-cold absolute methanol was taken. Cells were fixed with ice-cold methanol for 10 min. After that cells were washed with 1X PBS. Then cells were treated with PI containing PBS for 5minute at room temperature at dark. Then cells were washed with 1X PBS twice. 1 drop of glycerol was placed in a cover slide. Coverslips were taken carefully and then placed in a cover slide. Then confocal microscopy image of the cells was taken using ZEISS LSM600 confocal microscope.

4. RESULTS AND DISCUSSION

In this study CD and AuNP nano hybrid particules were aimed to be synthezied by using one pot solid state reaction method with fewer steps of the reactions and achive metal enhanced fluorescence to increase the fluorescence intenstiy of the CD. In the following step, bio-imaging ability of the synthesized solid state nanohybrid particles were investigated via confocal microscopy.

In the literature CD/AuNP has been produced via ex-situ reaction method. In this method AuNP were synthesized separately by using different methods such as the Turkevich method. Then AuNP were added into the reaction chamber as a reagent with carbon dot precursors. Then CD/AuNP nanohybrid particles were synthesized using hydro-thermal or solvothermal methods. However, the solid-state synthesis approach that has been investigated in this thesis does not require the initial synthesis of AuNP for nanohybrid production. AuNP nanoparticles in the solid state synthesis have been formed via the reverse Turkevich method [46].

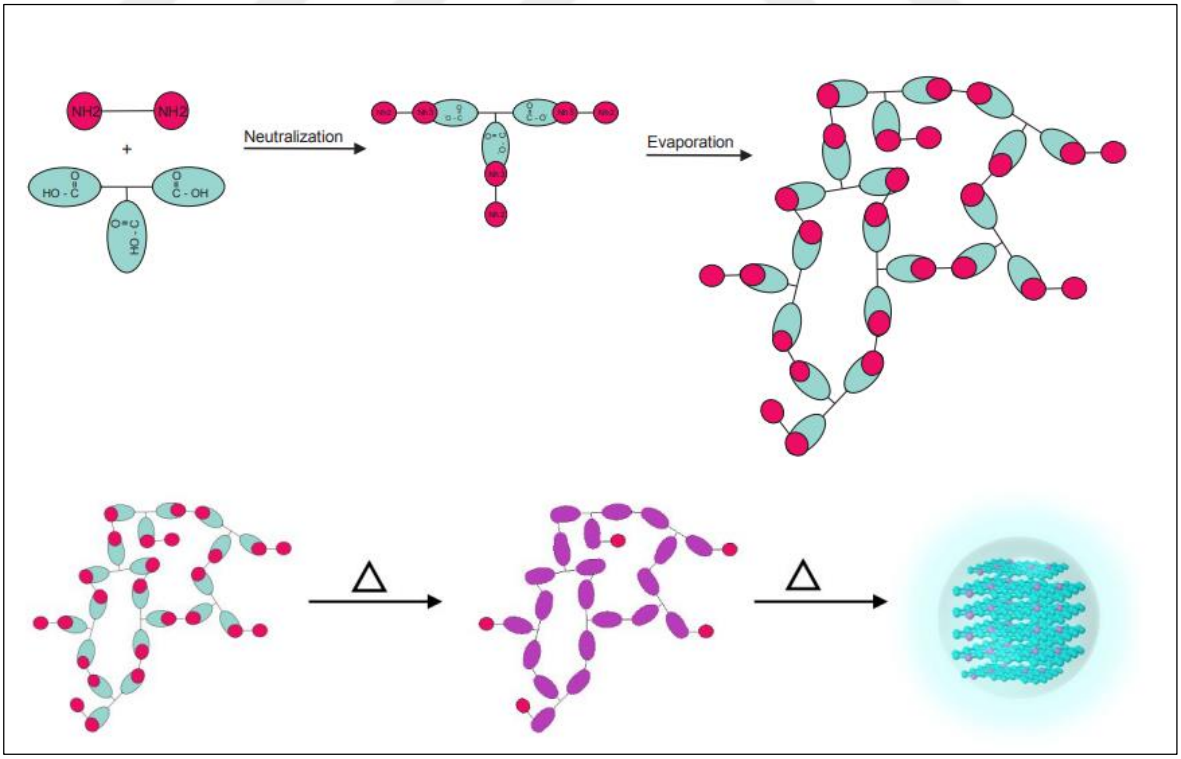

Figure 4.1 Formation of CA-EDA ion pair crystals with neutralization. Than in the evoporation of the solvent. As a result of the reaction N-doped-Cdot formation.

CD/AuNP nanohybrid particles are produced in the solid state either in the presence of pre-formed Au nanoparticles or Au nanoparticle precursor, HAuCl4. In both approaches, the mixture is first dried in an oven at 65°C and then heated up to 160°C for carbonization and gold nanoparticle formation at the same time. During the synthesis with the HAuCl4, nucleation, and growth starts in the same reaction chamber, so nano-hybrid structures have been formed as a result. The PL capacity of CD and AuNP nanoparticles could be altered via several conditions.

4.1 CHARACTERIZATION OF CQD/AuNP HYBRID

After the synthesis of SSNP, four different characterization methods were used to characterize the nanoparticles due to their physical properties and photoluminescence capacities. The methods used are DLS, UV-Vis spectroscopy, TEM and Fluorescent spectroscopy. From these methods, information was obtained about the dimensions of the particles produced with DLS and TEM. The photoluminescent capacities of the particles produced with fluorescent and UV-Vis were also agreed..

4.2 UNDERSTANGING THE GOLD NANOPARTICULE-FORMATION

Synthesized solid NP were analyzed using the UV-Vis light spectroscopy method. The result of UV absorbance data were analyzed for different purposes. To obtain the UV absorbance data, DI water was used as a blank solution because all of the precursors were dissolved in distilled water. All measurements were performed at the absorbance wavelength range between 200nm and 800nm. Before each measurement, a blank measurement has been carried out. To stay in the linear absorbance range, all measurements were performed using 1:500 dilutions with DI water.

Surface Plasmon Resonance (SPR) is the phenomenon that occurs in metal nanoparticles in this case gold nanoparticles. The main mechanism behind the SPR effect depends on the interaction of light with the free surrounding electrons on the surface of the gold nanoparticle. These electrons can be excited with light. Due to excitation, free electrons start the oscillation with a specific frequency which is directly related to excitation. Oscillations

in the electrons generate an electromagnetic field. This electromagnetic field could interact with light and it may lead to a reduction of the light intensity at a certain wavelength. This specific wavelength is also known as resonance wavelength and it has been related to the structural behavior of the nanoparticle [47].

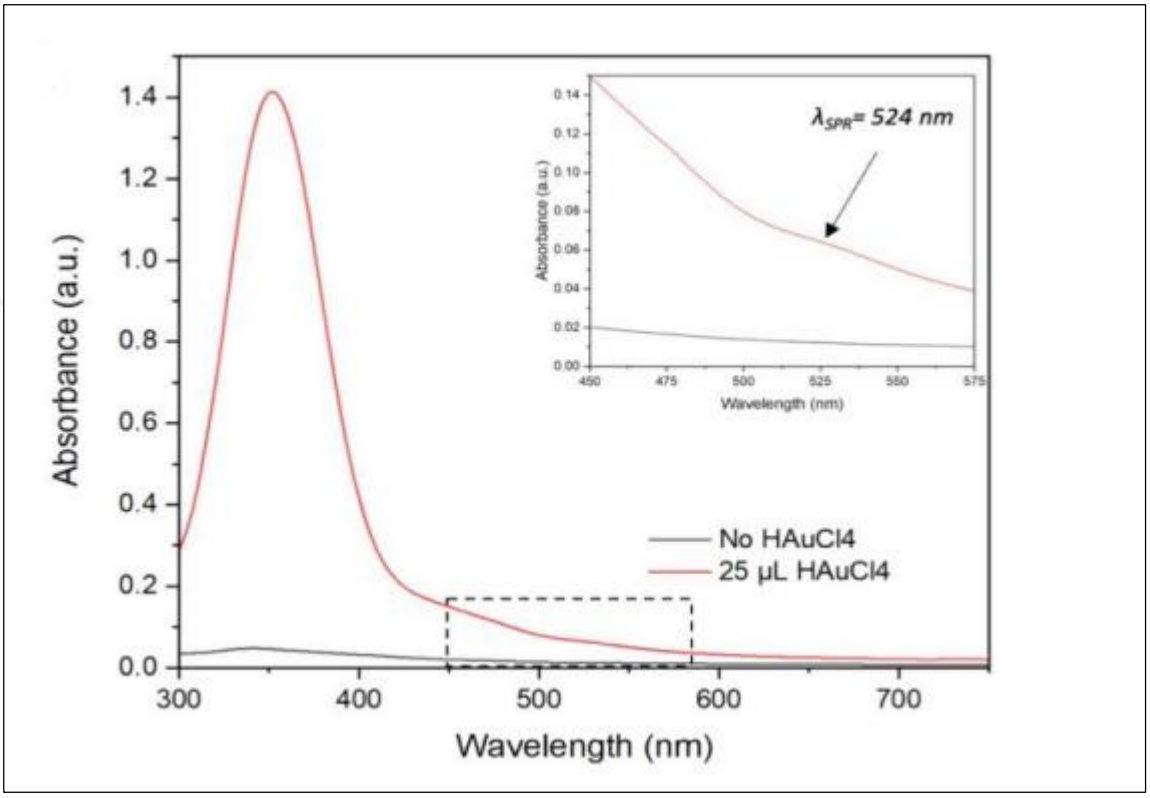

Figure 4.2 SPR wavelength comparing CD without $HAuCl_4$ and with 25ul $HAuCl_4$ containing synthesis.

Before using the nano-particular system with CD and AuNP. Nano hybridization formation in the reaction chamber should be analyzed. By considering the CD nature CD are not containing metal so they do not show any SPR effect. To understand the hybridization, UV-Vis absorption analysis has been conducted. CD absorbance spectrum shows that there is no specific reduction wavelength that occurs in the UV-Vis absorbance range. However with the addition of HAuCl4 in the reaction chamber, a specific absorption is observed at 524 nm due to the SPR effect of the gold nanoparticle formation. As a result of SPR analysis, there is extra data to understand that gold nanoparticles are formed as a result of the reaction with the addition of gold. However, this analysis does not say that the produced CD/AuNP showed metal-enhanced fluorescence. To understand metal enhanced fluorescence, all

produced solid-state syntheses CD and CD/AuNPs were analyzed by total UV-Vis absorption spectrum measurement and excitation-emission photofluorescence measurement

4.3 UV-VISIBLE ABSORBANCE MEASUREMENT

UV-Visible absorbance range spectrum measurement is important because it gives a general information about the excitation wavelength of nanoparticles. However, absorbance intensity does not directly relate to the PL capacity of the nanoparticle itself [48].

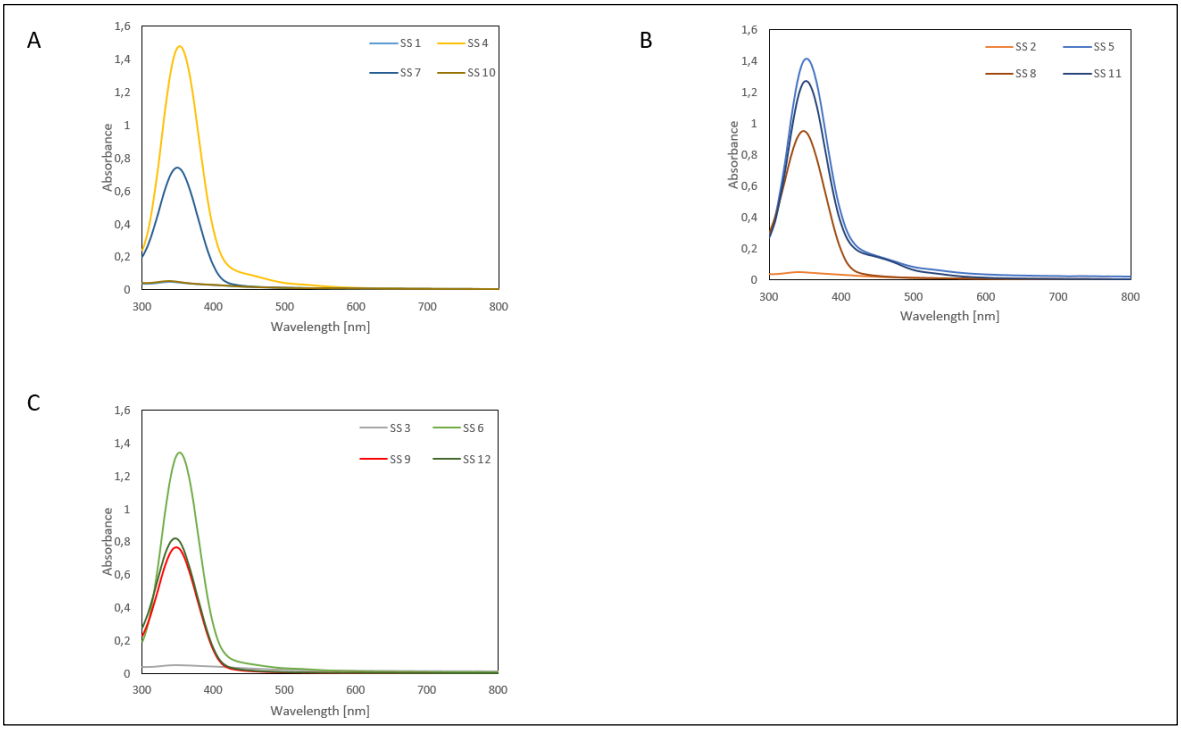

Figure 4.3 Total absorbance spectrum of the synthesized solid state nanoparticles. Figure 4.3 (a) shows that CA/EDA ratio 1 : 0.5 in terms of grams. Figure 4.3 (b) shows that CA/EDA ratio 1 : 1 in terms of grams. Figure 4.3 (c) shows that CA/EDA ratio 0.5 : 1 in terms of grams.

In the (Figure 4.3) represents the absorbance graph of all NPs synthesized with SS. Considering the spectra, all SSNPs show similar absorbance behavior as the maximum absorbance peaks appear close to each other. However, the maximum absorbance capacities change with the addition of HAuCl4 to the chamber. Because the 25 mM HAuCl4 addition reaction chambers in SS4, SS5, and SS6 show the highest absorbance values compared to other synthesized SS NPs. However, increasing the HAuCl4 concentration reduces the

maximum absorbance values of the synthesized NPs. However, the maximum absorbance values are greatly reduced in SS NPs without HAuCl4.

The SPR feature in SS NPs can be understood by examining the wavelength. In SPR, the maximum absorbance of the synthesized SS NPs does not change the wavelength, but as seen in (Figure 4.3 a), the effect of HAuCl4 addition on the SPR wavelength with a very small wavelength change can be observed in all nanoparticles containing HAuCl4.

When the absorbance characteristics of synthesized SS NPs were compared with commercial fluorescent dyes, it has been revealed that SS NPs show a similar absorbance wavelength as 4'-6-Diamidino-2-phenylindone, also known as DAPI dye. DAPI is used for DNA screening in biological environments such as ICC. DAPI has a maximum excitation wavelength at 358nm and the maximum emission at 461 nm [49]. Those SS NPs facing DAPI show a similar maximum excitation range, thus this information indicates that the absorbance spectra of SS NPs can emit blue light in the UV-Vis range.

4.4 MEASUREMENT EMISSION HEATMAP OF THE SSNP

The result of the emission wavelengths is measured with using fluorescence spectroscopy method. For measurement of the emission curve, all samples were diluted 1:500 with DI water. Also, DI water was used as a blank solution before measurement each time. To determine the maximum wavelength of the intensity, the samples were emitted at different wavelengths and the fluorescence intensity was measured at each emission. To determine the maximum emission wavelength, samples were illuminated at different wavelengths and the emission wavelength and intensity were recorded. Then the results were analyzed for different application areas, like bioimaging.

After UV-Vis absorption spectrum measurement, the effect of HAuCl4 addition on the emission properties of SSNPs at the emission wavelength is not fully understood. Therefore, emission wavelengths were measured using fluorescence spectroscopy method and the effect of HAuCl4 addition on emission wavelengths was investigated. The main reason for making this comparison is primarily to understand the effect of HAuCl4 addition on the emission spectrum of SSNPs. Also, due to the SPR effect, if the maximum emission wavelength is in the SPR region range, the gold-containing SS NP'S should create an undesirable internal

filtering effect as it can reduce the maximum PL capacity. The main reason for this is that if HAuCl4 containing SSNPs emits light at 524 nm, this emitted light is directly absorbed by the gold, so the emitted light intensity can be reduced by the HAuCl4 containing SSNPs itself.

In addition, studies have shown that CD size directly affects the maximum emission wavelength. As the CD size increases, the emission shift of the CD moves from the UV range to the Near IR range. For example, 0.5nm CD emits light in the UV range of the spectrum. By increasing the size from 1 to 1.5 nm, CD can emit light in the blue region of the light spectrum [50].

The fluorescence capacity of CD is directly related to the QCE effect. Thus, the measurement of absorption emission spectra becomes even more important in this way. In addition, the QCE effect explains the maximum fluorescent emission shifts of CD [51,52].

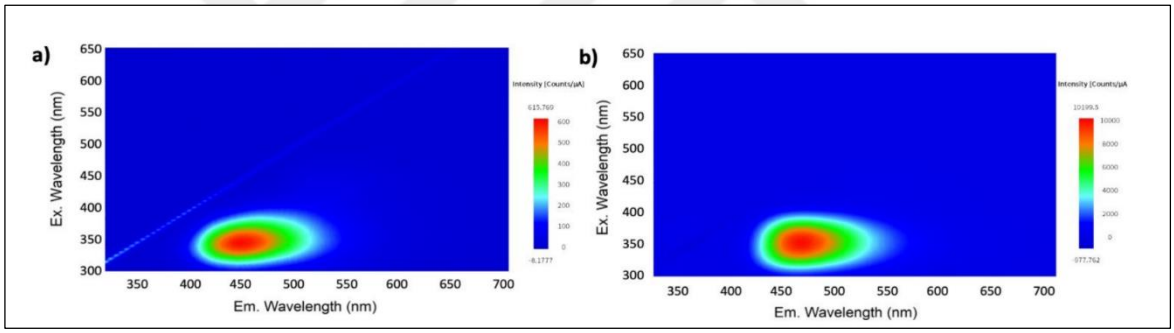

Figure 4.4 (a) excitation emmission heatmap SSNP without $HAuCl_4$. Figure 4.4 (b) excitation emmission heatmap SSNP with 25ul $HAuCl_4$

Looking at the excitation-emission heatmap (EEM) of the CD emission center, it is located at 447nm, which is the center of the blue emission spectrum. At 457nm, the center of the blue emission spectrum, there is 25 mM HAuCl4 containing maxiumum emission point. Thus, the results show that the addition of HAuCl4 does not greatly change the maximum emission wavelength. Only minor changes occur in the system. Also, when comparing the synthesized SSNPs with commercial DAPI, they show similar PL properties due to their PL capacity. This means that SSNP implementation can be done directly using the DAPI channel; this ensures that the use of the SSNP system can also be used for bioimaging systems. Visualization of the SNP can be done using the DAPI channel itself in confocal microscopy imaging.

4.5 EMISSION WAVELENGHT COMPARISON OF THE SSNP'S

After EEM analysis, it was shown that the addition of HAuCl4 did not change the maximum emission wavelength of the SSNP, but their maximum intensities should be properly analyzed. On the other hand, it may be possible to increase the PL intensity of SSNPs by comparing CD with energy transfer resonance due to metal-enhanced fluorescence (MEF). Since the excited electrons in the CD can interact with the surface-free electrons in the gold nanoparticles, this interaction creates a specific resonance. This resonance significantly increases the fluorescence capacities of CD [54].

On the other hand, understanding the emission behavior can give a general idea of the PL capacity of the product. This should be done for all produced fluorescent NPs because in commercial fluorescent dyes each specific dye has significant EEM. Therefore, manual or program-based compensation is required before using SSMPs with other commercial dyes.

PromoFluor label	Adsorption maximum [nm]	Emission maximum [nm]	Excellent alternative to	Laser excitation source
PF-350P	338	436	Alexa Fluor® 350, AMCA, AMCA-X	Argon Laser, UV-light
PF-405	400	420	Alexa Fluor® 405, Pacific Blue™, Cascade® Blue	Blue diode laser, Violet 405 krypton laser
PF-415	418	467	Pacific Blue™, Cascade® Blue	Blue diode laser, Violet 405 krypton laser
PF-488P	490	516	Fluorescein (FITC), Alexa Fluor® 488, Cy2	Argon 488 blue-green laser
PF-505	505	530	RhodamineGreen	Argon 488 blue-green laser
PF-532	539	561	Alexa Fluor® 532, Tetramethylrhodamine (TMR, TRITC)	Nd:YAG laser
PF-546	551	572	Alexa Fluor® 546, Tetramethylrhodamine (TMR, TRITC)	Helium-Neon 543 green laser
PF-555P	557	571	Alexa Fluor® 555, Cy3, Tetramethylrhodamine (TMR, TRITC)	Helium-Neon 543 green laser
PF-568	580	598	Texas Red, Alexa Fluor® 568, Cy3, Rhodamine Red™/Rhodamine B dye	Helium-Neon 594 laser, Ar-Kr mixed-gas laser
PF-594	594	615	Texas Red, Alexa Fluor® 594	Helium-Neon 594 laser
PF-633P	635	658	Alexa Fluor® 633	Helium-Neon 633 laser, Red diode 635 laser
PF-647P	654	672	Alexa Fluor® 647, Cy5, Allophycocyanin	Krypton-Argon 647 laser
PF-670	673	694	Alexa Fluor® 660, Alexa Fluor® 680, Cy5.5	Helium-Neon laser
PF-680	690	709	Alexa Fluor® 680, Cy5.5	Helium-Neon laser
PF-700P	706	731	Alexa Fluor® 700	Far-red diode lasers, xenon-arc lamp, dye-pumped lasers
PF-750	748	772	Alexa Fluor® 750, Cy7	Far-red diode lasers, xenon-arc lamp, dye-pumped lasers
PF-770	769	796	Alexa Fluor® 750, Cy7	xenon-arc lamp, dye-pumped lasers
PF-780	783	800	NIR dye	xenon-arc lamp, dye-pumped lasers
PF-840	844	884	NIR dye	xenon-arc lamp, dye-pumped lasers
PF-865	863	896	NIR dye	xenon-arc lamp, dye-pumped lasers

Figure 4.5 Commercial fluorescence dyes especially for flow cytometry and ICC [55].

Understanding the overall emission range of the produced SSNP is important for designing experimental setups for bioimaging studies with SSNPs. Excitation and emissions of dyes must not overlap. The main cause of this overlapping excitation and emission can be non-specific emissions that can create a dirty background in the environment, or non-specific signaling or non-specific sensing that can lead to false results. For example, using 25mM HAuCl4 containing SSNP together with FITC may cause false results, as the maximum emission wavelength of FITC directly overlaps with the SPR region of SSNPs. Thus, it may cause false results as it may increase the detection limit in the environment. Also, SSNPs cannot be used with Alexa Fluour 405, Pacific blue CoroLite 488 and DAPI due to their similar EEM.

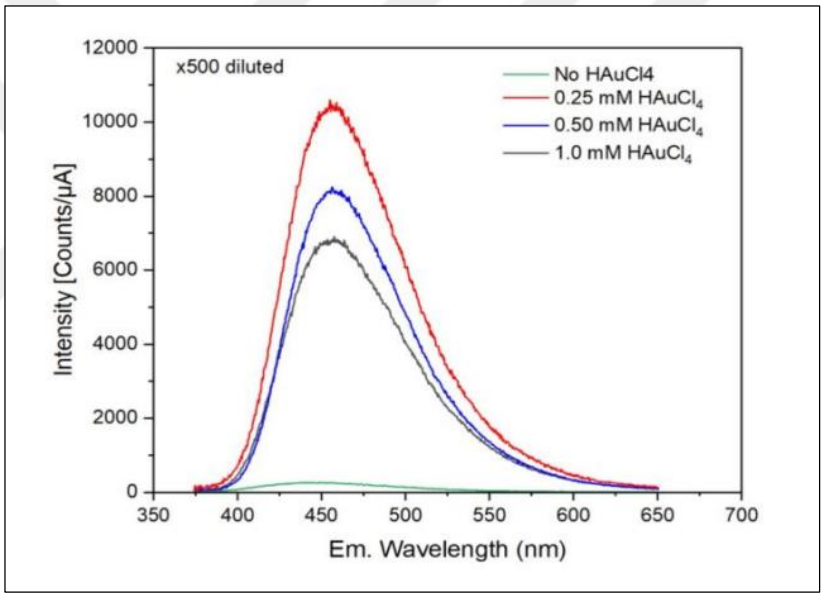

Figure 4.6 Metal enhanced fluorescence emission comparison in SS2, SS5, SS8 and SS11

In the (Figure 4.6) shows the hybridization of CD and AuNP in the reaction chamber, observing the SPR peak in UV-Vis absorption. On the other hand, an increase in PL density is observed due to the MEF of synthesized SSN Ps with similar CA/EDA ratios with the addition of HAuCl4. To understand the MEF effect, SS2, the only reaction containing the CD precursor, must be compared with other SS reactions. As a result of the measurement made considering this situation, it is shown that the addition of HAuCl4 to HAuCl4 doped SSN particles significantly increases the emission wavelength when the SS nanoparticles are excited at the maximum absorption wavelength. But the real question is whether increasing HAuCl4 in the reaction by more than 0.25 mM reduces the PL capacity compared to SS5. Several reasons can be explained for this situation. First, due to stoichiometric equilibrium,

the concentration of HAuCl4 in the reaction chamber should be increased and the amount of CD precursor should be increased. Another reason is the two main reactions that occur in CD synthesis and CD production and AuNP formation. The increase of CD precursors also increases the nucleation and growth rate of carbonization, but at the same time, hybrid formation occurs during the reaction. Increasing HAuCl4 concentration may cause the degradation of CD precursors, especially citric acid, and may be effective in the nucleation of gold and carbon nanoparticles [56].

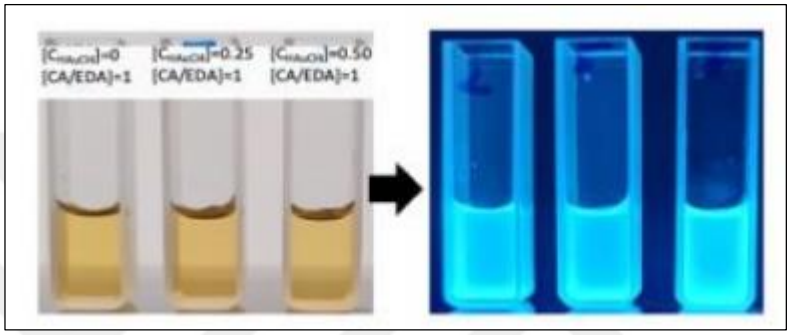

Figure 4.7 Light emission comparison with naked eye of the produced SSNP's with different HAuCl4 concentration under UV light.

When looking at the SSNPs synthesized under UV light with a wavelength of 300nm, luminescence was observed inside the containers containing nanoparticles. As a result of the observations, nanoparticles do not show significant changes for the human naked eye. Several conditions can affect this result. First, the solutions are not diluted in this analysis, so differences in brightness with higher concentrations cannot be discerned with the naked eye.

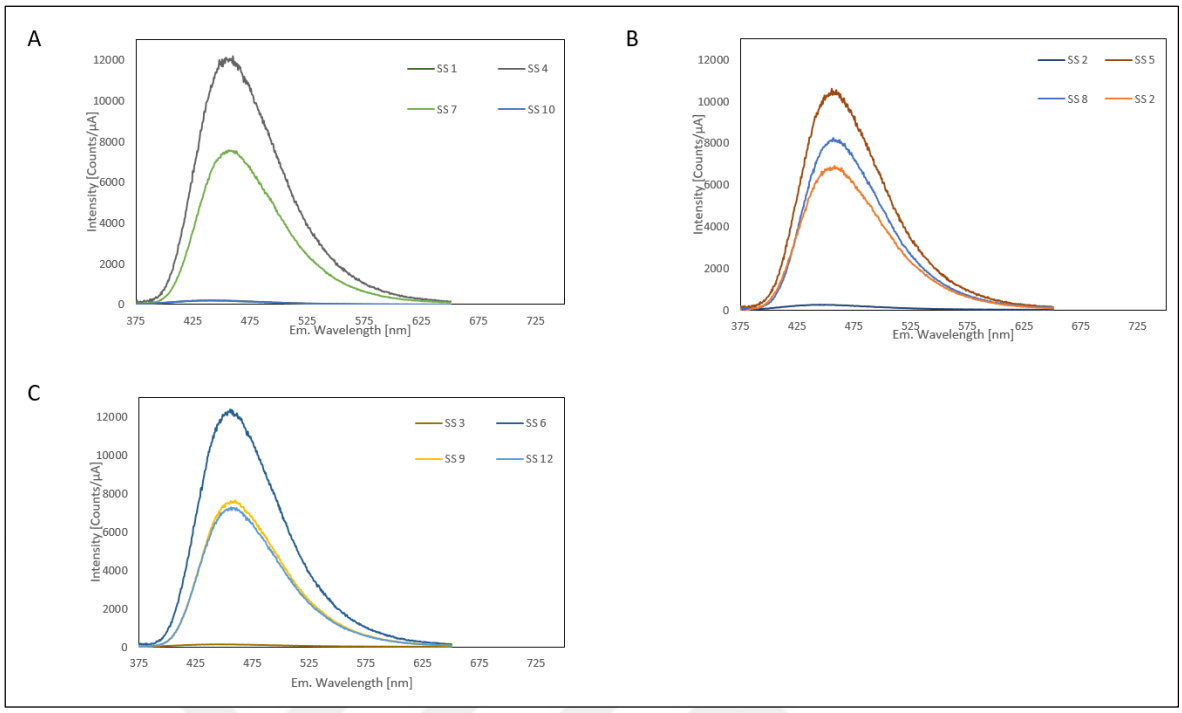

Figure 4.8 Emission comparison of the synthesized SSNP's due to their $HAuCl_4$ amount with CA/EDA 1:0.5 in Figure 4.8(a) , CA/EDA 1:1 in Figure 4.8 (b) and CA/EDA 0.5:1 in Figure 4.8 (c).

After comparing the MEF depending on the amount of HAuCl4, it should also include the effects of CD precursor concentration. Comparison of the CA/EDA ratio under fluorescence does not directly affect the maximum light emission in the synthesized SNP. Because, for example, when comparing the maximum emission of SS1, SS4 and SS7, and SS10, they emit light of similar intensity. A similar result emerges when compared with other CA/EDA ratios. Measurement of PL density for the entire SSNP shows that drastic PL density changes in the synthesized SSNP are directly related to the MEF effect. Hybrid formation increases the PL density of the synthesized NPs.

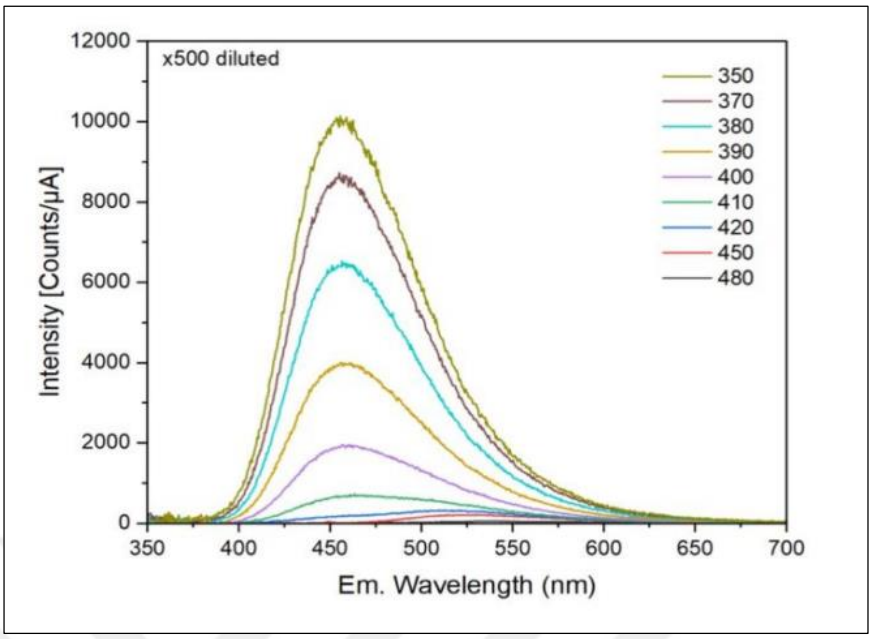

Figure 4.9 SS5's PL intensity with different excitation wavelengths merged results.

In the PL mechanism when the NP is initiated with higher energy light fluorescence emission is observed with the lover energy spectrum of the light. The EEM maps are giving general information about the PL wavelength of the synthesized SSNP but it does not give excitation-emission wavelength comparisons so general analyses should be made to understand the differences between different excitation and emission intensity of the SSNP.

In the (Figure 4.9) is showing that synthesized SS 5 is showing the maximum PL intensity in 350nm excitation. This result is expected because SS5 is showing maximum absorbance at also a similar wavelength which is 352nm. However, decreasing the light energy/increasing the excitation wavelength is decreasing. Maximum light emission is observed at 455nm which also means that produced CDs are considered as blue CDs.

4.6 SIZE ANALYSES OF PRODUCED SSNP'S

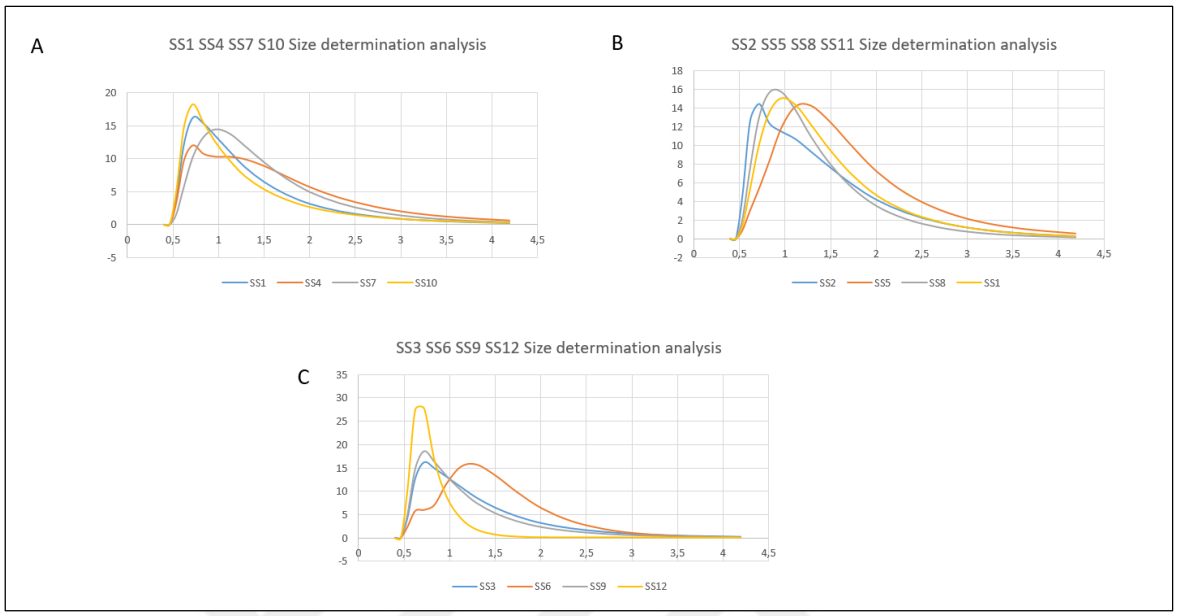

Figure 4.10 Size analyses and comparison of the synthesized SSNP's due to their $HAuCl_4$ amount with CA/EDA 1:0.5 in figure 4.10 (a), CA/EDA 1:1 in figure 4.10 (b) and in figure 4.6 (c) CA/EDA 0.5:1

In the (Figure 4.10) shows that DLS dimensional analysis of both produces SSNP synthesis. By analyzing the results, SSNPs generally show similar size distribution of 2±1.5 nm in a range. When producing nanoparticles in the solid state method, minor changes may occur in the reaction chamber as all carbonization and nucleation and growth take place in a very small place in the medium compared to liquid phase hydrothermal synthesis. One of the questions in this synthesis is whether the mono inequality of the produced nanoparticles will increase and decrease the precursor vacancies. The results show that all synthesized SNPs show similar size behavior. Also, comparing the PL density of SSNPs provides a second check of the size of the SSNPs produced.

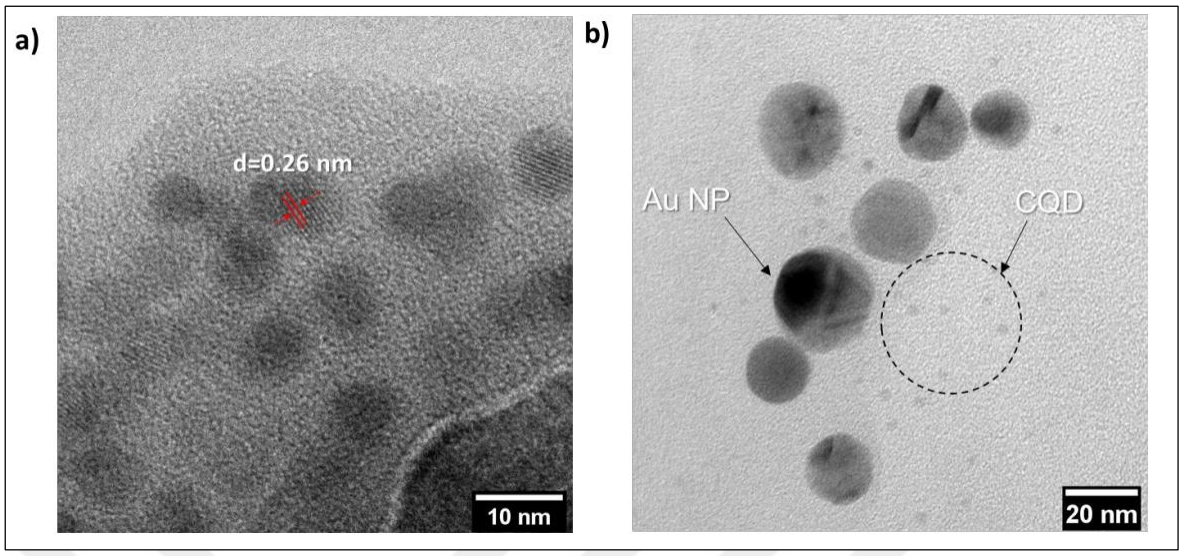

Figure 4.11 TEM image of the synthesized nanoparticles. Figure 4.11 (a) showing that closed image of CD only and Figure 4.11 (b) showing that hybrid structure of produced CD/AuNP in SSNP reactions of TEM image

In the (Figure 4.11) show the TEM image of the synthesized nano-hybrid structures. In (Figure 4.11 a) shows CD in hybrid formation. In the CD structure, the single line mesh spacing was measured as 0.26nm. However, bare analyzes of CD/AuNP nano-hybrid formation size are 7 ± 1 observed when looking at (Figure 4.11 b). Also, (Figure 4.11 b) shows that CD surrounds the AuNP surface. Figure 20 (b) shows that there are more than 1 hybrid construct. Also, looking at (Figure 4.11 b), unconjugated crystal structures of CD are seen in the minority. However, PL analyzes show that hybrid structures do not affect PL capacity. Due to the reaction kinetics, small amounts of unconjugated free CD formation are also expected.

4.7 *IN-VITRO* EXPERIMENTS

The second part of this study is to apply the synthesized nanoparticles in an in vitro cell culture model to understand the bio-imaging properties. In addition, the bio-imaging properties of healthy and different cancer cell lines will be compared to determine which cancer type is more suitable for the use of the CD /AuNP hybrid system. Prior to the application of CD /AuNP's, the proliferative effect and cellular toxicity were investigated. For to understand the differences in bio-imaging and cellular cytotoxicity different cancer

cell lines and healthy cell line were chosen for that reason. Different cancer model cell lines for A549 is lung, MCF-7 is breast and Panc02 is pancreatic carcinoma. They are both different types of cancer. Due to the metabolism of the cancer after the treatment of SSNP's possible outcome could be different. So that finding the most suitable organ or cell type is crucial for bio-imaging properties is important. Also HDF is common healthy cell line for also used as general control cell line. Using healthy cell line is important because for any purposes of the produced NP especially for bio-imaging used products are needed to be safe and non-toxic for healthy cells.

4.8 CELLULAR CYTOTOXICITY DETERMINATION OF PRODUCED SSNP'S

To understand cellular proliferatio MTS cellular proliferation assay was used. For the treatment SS (2,5 and 8) is selected considering their absorbance and intensity values and does not showing aggregation. For the SS reaction, 3 different replicates were selected with their HAuCl4 concentration to understand whether gold concentration has a positive or negative effect on cell proliferation. To understand cellular proliferation, the MTS assay was used. In the MTS assay, cells were treated with different concentrations of NP ranging from 7.8Um to 3500Um. The cells were treated for different time periods such as 24, 48 and 72 hours. When cells were treated, all NP were NP were mixed in fresh medium. For the negative control, only a fresh medium change was performed. For understanding the cell death or inhibition of cellular growth also known as positive control. For to understand the inhibition effects of the SS CD/AuNP nano hybrid particles in the cell growth all cells in the positive control were treated with 10% dimethyl sulfoxide (DMSO). After treatment of the cells, the data were analyzed using Excel.

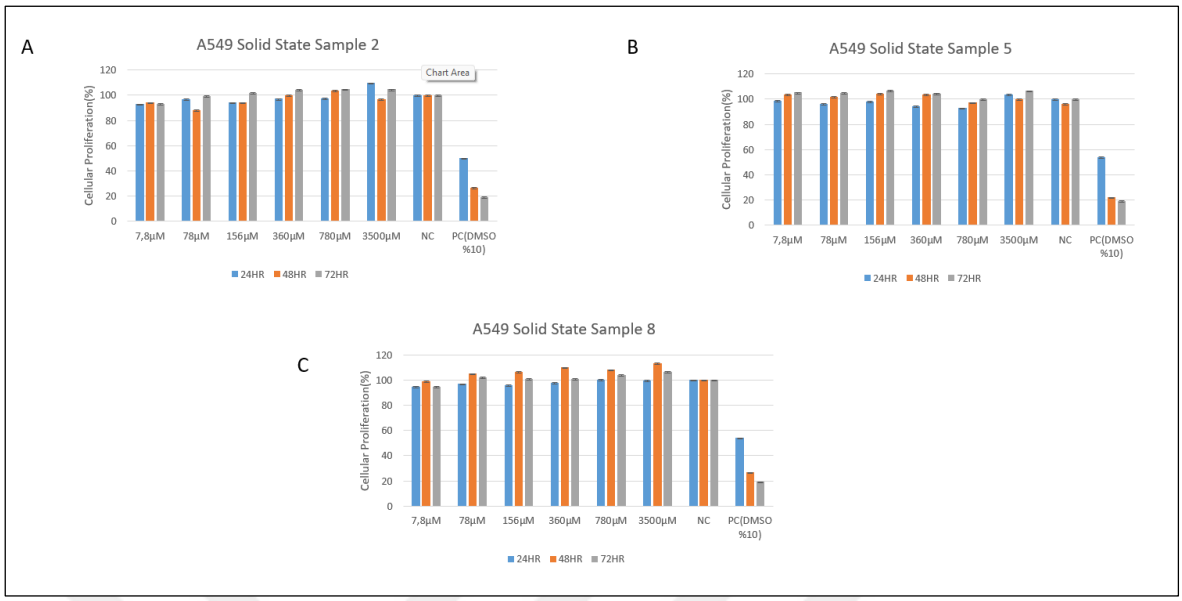

Figure 4.12 MTS assay for A549 in treatment of SS2 in Figure 4.12 (a) SS 5 in Figure 4.12 (b) and SS 8 in Figure 4.12 (c) including with standard deviation.

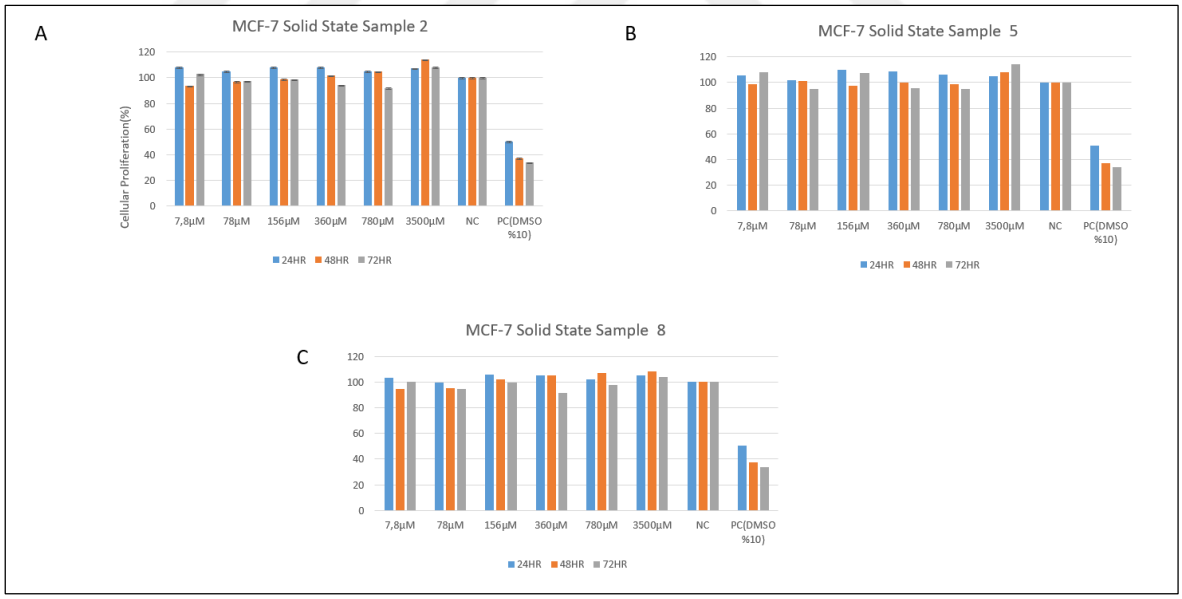

Figure 4.13 MTS assay for MCF- in treatment of SS2 in Figure 4.13 (a) SS 5 in Figure 4.13 (b) and SS 8 in Figure 4.13 (c) including with standard deviation.

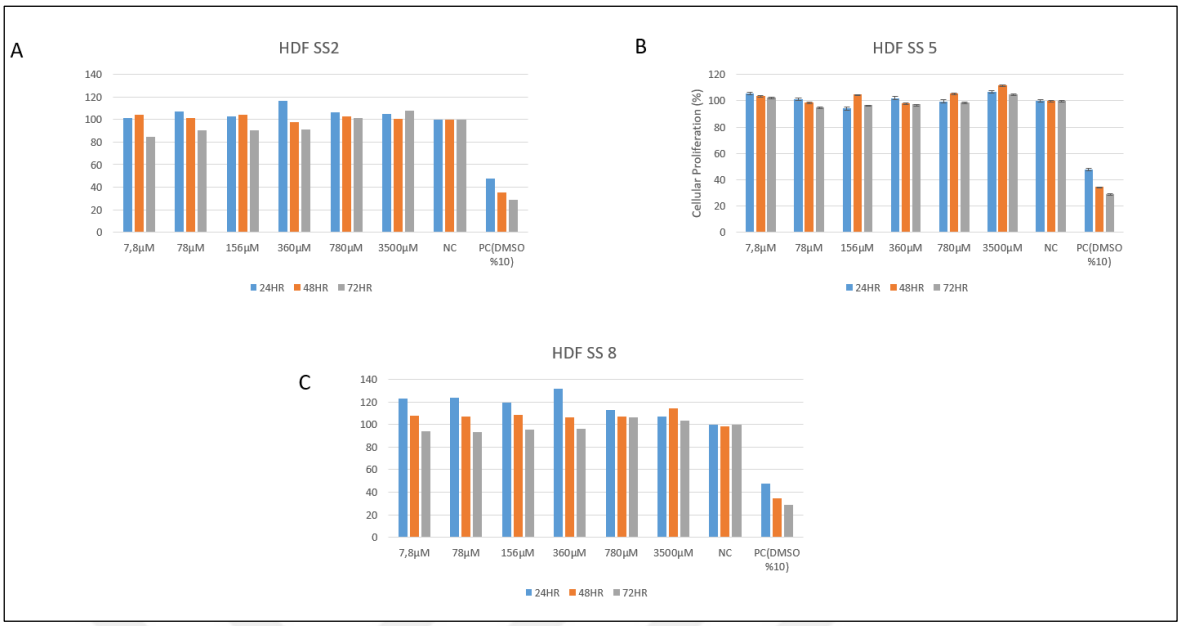

Figure 4.14 MTS assay for HDF in treatment of SS2 in Figure 4.14 (a) SS 5 in Figure 4.14 (b) and SS 8 in Figure 4.14 (c) including with standard deviation.

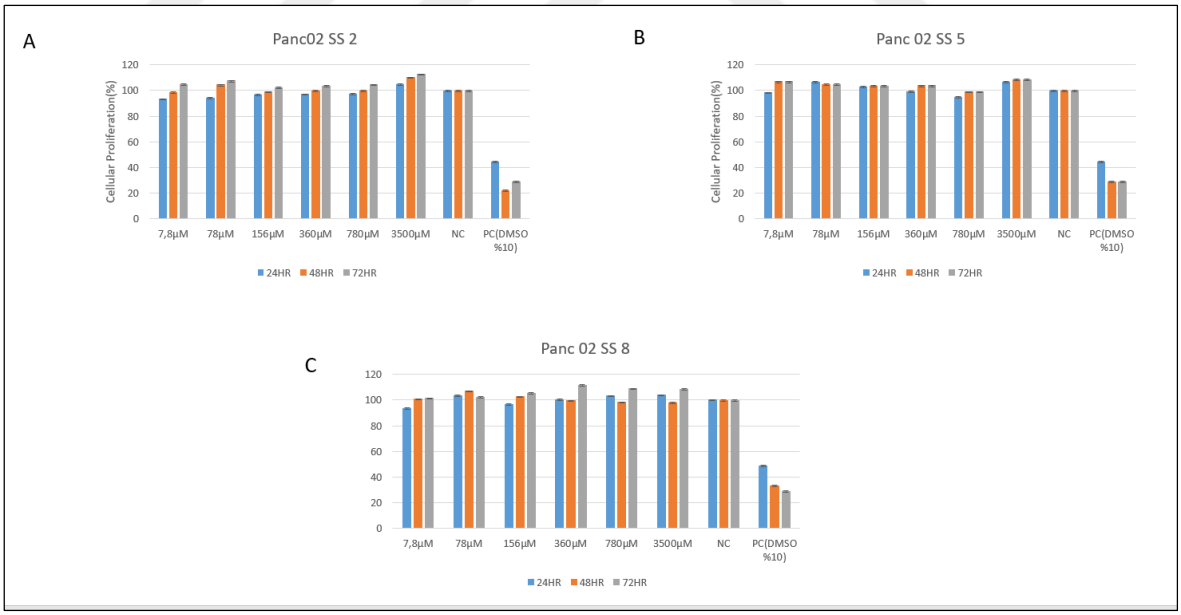

Figure 4.15 MTS assay for Panc02 in treatment of SS2 in figure 24 a SS 5 in Figure 4.15 b and SS 8 in Figure 4.15 (c) including with standard deviation.

Before the doing of MTS assay minimum of 3 wells were inoculated with cells to reduce the experimental error of the manual seeding process. Because manual micropipettes may be able to have some minor mistakes during the experiment or cell suspension stock could be

not mixed well. So that 3 replicates are important for that step. Also in every reading all of the wells were compared with each other to control is there any major significant changes have been occurring in each treatment. If the standard deviation of the 3 wells more than 5 experiments were replicated respectively.

To analyze the experimental data proliferation absorbance of the control group was taken %100 on each day of treatment. Then the other proliferation data was analyzed due to the comparing with the control group itself.

MTS assay is a common method for evaluating the cytotoxic effect or proliferative effect of various molecules on cells [57,58]. AuNP's are considered non-toxic, however, finding the optimal treatment dose for bioimaging properties is quite problematic. The main reason is that cells may not be able to tolerate the AuNP doses required for bioimaging properties and proteins involved in cell proliferation may be damaged [59]. The main toxicity is due to the structural charge of AuNP and the surface-active molecules [60]. To understand the proliferative effect of the synthesized SSNP cells were treated with CD /AuNP for several days. The reason is that AuNP in different doses could be toxic in the cellular environment, because the ingestion of AuNP could damage the cell membrane. Also, the treatment dose of SSNP system is important to optimize the bioimaging properties [61]. MTS Assay provides the result with the change of tetrazolium salt to formazan compound on the ratio of mitochondrial ATP synthesis. Thus, the MTS assay can generally indicate the proliferation of the cell in cell culture [62]. For this purpose, both cell lines were tested with different doses. In addition, both cell lines were tested over different time periods to understand the late onset reduction in proliferative effect. To this end, both cells were tested over 24, 48, and 72 hours to understand the proliferative effect of the synthesized SSNP nano-hybrid particles. The results show that treatment of SS series in a range of (7.8um to 3500um) shows no significant differences in proliferative effect. Minor changes in proliferation could occur in the MTS assay because all cells were seeded using a multichannel micro pipetting system with a large stock solution. Any time minor pipetting errors are made to alter cell concentration, the differences in the MTS assay can be amplified [63]. Also in the MTS formazan formation directly related with alive and metabolically alive cell number in the well plates. And cells are divided by log2 scale than 100 cell differences in wells could significantly affect the overall result in the chamber.

To cross-check the treatment dose determined for the bioimaging system, cells were also examined for apoptosis. Apoptosis is a phenomenon that controls cell death. It can be triggered by various factors, such as FAS-FAS L interactions or high NO levels in the cell, or by blocking various signaling pathways in the cell. Apoptosis alters cell morphology and requires the activation of various signaling pathways, such as caspases. Necrosis is caused by damage to the cell membrane by chemical or passively transported molecules. During necrosis, cellular compartments are ejected and cell swelling occurs [64]. Annexin-v staining is one of the simplest methods to analyze apoptosis and necrosis in cell cultures. The results of this assay provide information about the apoptosis level in the cell culture and the necrosis ratio [65,66].

Both cells were treated with a dose of 780Um, which is the main reason that this is the highest dose suitable for bio-imaging applications because when the higher dose was applied to the media color of the media has been drastically changed from pink to color of yellow. Cell culture mediums are generally containing phenol red in their chemical composition. Phenol red is a general PH indicator it shows the general PH changes in the solution. Under the normal condition cell culture medium have a unique reddish to pink color which is showing that PH is around 7.2 however after adding more than 780nm of SSNPs in the medium. PH of the environment drastically turns into an acidic environment. It does not give any damage to the cellular proliferation due to the MTS assay however MTS assay is not enough the understand the effects of the PH changes in the cell metabolism. So that 780um SSNP’s was used for that reason in the apoptosis assay [67].

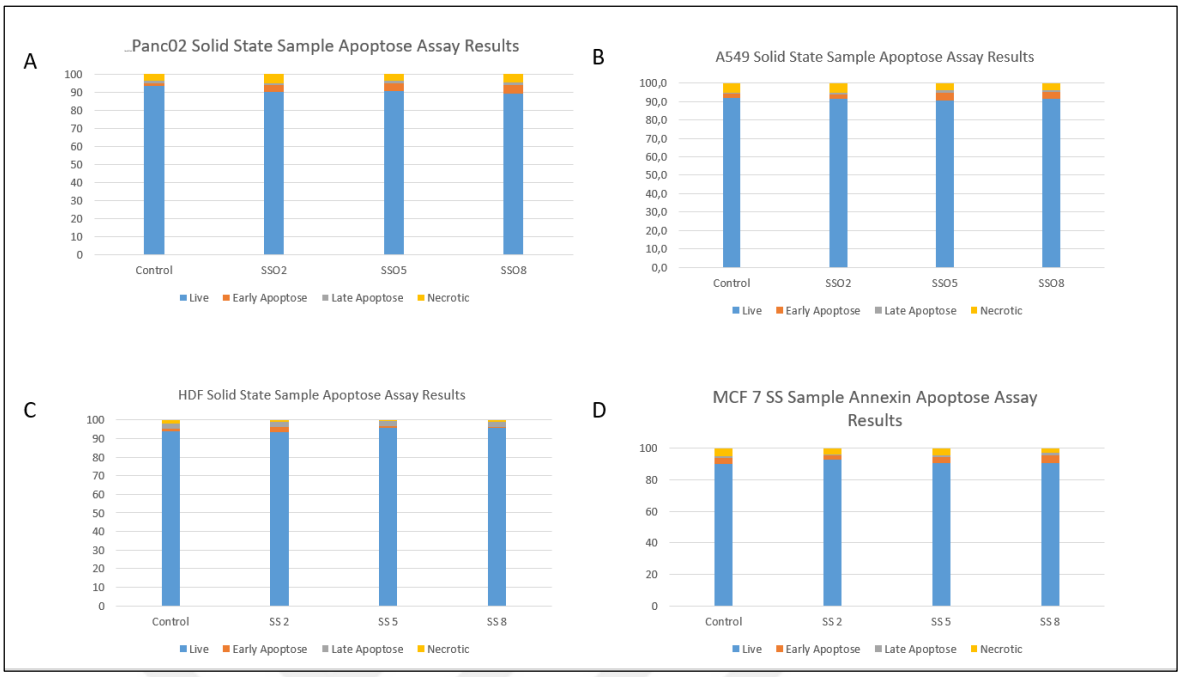

Figure 4.16 (a) result of the apoptosis assay of Panc02 cells. Figure 4.16 (b) result of the apoptosis assay of A549 cells. Figure 16 (c) result of the apoptosis assay of HDF cells. Figure 16 (d) shows the apoptosis assay of MCF -7 cells.

Based on the flow cytometric analysis, 20000 cells were read in a selected gate at each reading. In addition, apoptotic and necrotic provisions were made with unstained cells before reading to understand cell localization. In the bar graph, the blue colored lines represent live cells in a given population. The orange lines represent the early stage of apoptosis stained only by FITC-labelled annexin V. Yellow lines show propidium iodide staining indicating necrotic cells in the population. Grey-colored bars represent the late stage of apoptosis stained by FITC-labelled Annexin V and PI together.

Results of the apoptotic assay show that by comparing the cellular conditions with the control group all of the treated groups are showing similar conditions just like the control group in the treatment protocol. In the cellular growth conditions, approximately %90 of the cells were not stained by annexin or PI. Which means that they are alive cells. Because annexin is a representative bio-marker for apoptotic conditions in the cellular dead. So that if the cells were not stained with annexin it means that they are alive.

Also PI is the dye that could able to stain DNA or RNA in the cytoplasm only if the cells were in necrotic or apoptotic conditions. In the necrotic conditions, cells were damaged

physically so that their cellular bilayer contains different junctions. PI could easily penetrate with this junction PI could easily penetrate the intracellular membrane of the cell. Which determines necrosis. However, during experimental conditions small percentage of the cell could be dyed by PI also they could be necrotic or dead. Considering all of these as a result of the annexin apoptotic cell determination assay. SS 2, SS 5, and SS 8 does not show intracellular or extracellular apoptotic/necrotic damage to the cell

4.9 BIOIMAGING STUDY

After the cellular proliferation and cellular cytotoxicity detection assay, defined doses of the both HTB and SS series of the reactions were monitored for the bio-imaging capacity in-vitro experiment. Confocal microscopy has been utilized for this purpose To detect the CD/AuNP hybrid particles, the laser of the confocal microscopy was set to DAPI channel 405nm emission. Since confocal microscopy can not give a bright field image, all the cells were dyed with propidium iodide (PI) solution to understand the cellular localization in the slide. PI binds DNA/RNA in the cells so that it may give the exact image of cellular morphology and cellular localization in the slide.

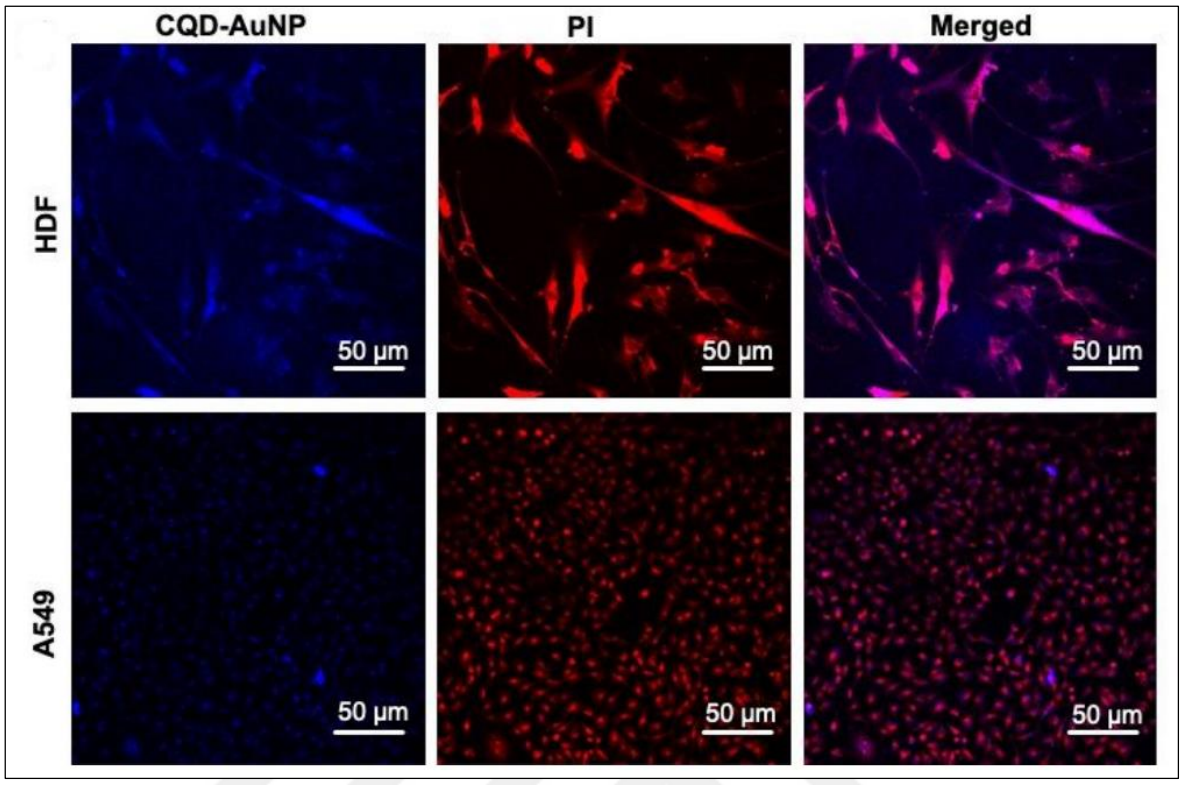

Figure 4.17 Confocal microscopy images of HDF and A549 cells. In the CD/AuNPchannel, both cells are showing DAPI channel results which is showing the cellular uptake of the synthesized SS5 CD/AuNP nano-hybrid system with a scale bar. In PI channel directly shows cellular localization for both cells. In merged channel is showing the localization of SS5 particular and PI in the same picture

In the (Figure 4.17) shows the imaging performance of SS5 in the DAPI channel. After the cells were treated CD/AuNP for 24hr after the cellular attachment was done. As shown in (Figure 4.17), nanohybrid structures have stained healthy cell, HDF more distinctively than lung cancer cell line A549. The merged image is showing that the uptake of the nanoparticle from the cell is proper level and cellular detection was made successfully.

The results show that HDF and A549 cells are suitable for staining with the SS5 system. Confocal microscopy results show that HDF cells are the most suitable for bioimaging in this study. A549 cells were also detectable by confocal microscopy. However, the main goal of this study is to detect cancer cell lines using CD /AuNP, and the results show the opposite. Besides this result, the main objective is also acceptable. The main reason is that in the cell culture study, the healthy cells were exposed to more light than the cancer cell lines, which

means that the darker field represents the cancer cell lines. On the other hand, the metabolism of the cancer cell lines can digest the nanoparticles produced. Since all cells in this study were treated for 24 hours, cancer cells can be detected in the literature after only 2 hours of treatment [68]. This means that the entire experimental setup needs to be repeated for other treatment times such as 2 hours, 4 hours, and 12 hours. The main reason for this experiment is to find the optimal time for detection, and with this experimental setup, MCF -7 and Panc02 could also be used for detection however in this experimental setup MCF-7 or Panc02 does not show any emitted light in the confocal microscopy. To increase the selectivity inoculation of the SNP's time can be directly arranged 2-4 hours before the experiment then the outcome of the confocal image could be reversed by decreasing the treatment time. Besides that after finding the most optimal time for bio-imaging treatment for cancer cells. Co-culture studies should have must do respectively with the healthy or control cell line with the cancer cell line. Uptake of SSNP's can be distinguished by using live cell imaging dyes and absorption of the SSNP's can be compared with both cell lines. As a result of it cancer cell detection can be made by only arranging the treatment time.

Also for the fixation protocol for confocal microscopy cells were fixed using absolute methanol. In that situation, absolute methanol also could able to destroy the CD/AuNP Nano hybrid particles in the cells. Because every cell has a different unique structure different fixative may be used for that manner such as %4 paraformaldehyde or acetone methanol mixture may be used for that manner.

To understand the uptake mechanism of SSNP the cells must be treated with serum-free media, low-glucose media with serum, and low-glucose media without serum. In this experiment, body conditions are mimicked when the stomach is hungry and when it is full. Thus, different body conditions are analyzed to understand the general uptake mechanism for the SSNP'S. Also, different stress conditions should be needed for further studies such as reactive oxygen stress conditions or different chemical stress conditions.

Also, during the experiment, the confocal microscope is not able to determine the wavelength of laser excitation because all particles have the highest PL intensity at 350nm excitation. However, in this experiment, the cells were observed at 405nm, which corresponds to the emission radius of DAPI dye excitation. DAPI is the common nuclear dye in biology, so the DAPI channel can be found in all different fluorescence and confocal microscopes [70]. Thus, the development of the SSNP's system with a similar PL capacity

to DAPI will increase the general use of the nanomaterial. It is possible that the SSNP's system is not properly excited during confocal microscopy, resulting in a decrease in the PL capacity of the system. To increase the fluorescence capacity of the SNP's system, the excitation-emission range must be designed to increase the detection limit of the system.

No preliminary work is required for SSNP's nano-hybrid particles, whereas cell tracking dyes present several problems, such as their low reproducibility and the need for several optimizations before use [70]. The application of SSNP's nanohybrid particles is quite straightforward. Also, the SSNP's system does not require significant pre-optimizations. Mixing SSNP's nanohybrid particles with fresh culture medium provides sustained stabilization. Cell tracker dyes also need to be applied at the beginning of the cell seeding process. Each time a cell divides, the fluorescent emission from the cell tracker is shared directly across the cell division because the dyes are shared with two daughter cells during cell division [71]. Therefore, SSNP's nano-hybrid particle system is dissolved in the medium, so each divided cell could absorb from the medium, so photofluorescence levels do not change directly day by day. On the other hand, cell tracker dyes show toxic effects on cells because too long application causes cellular cytotoxicity. Therefore, the application of cell tracker dyes must be optimized in advance [72]. However, the CQD-Au NP system shows no proliferative or cytotoxic effects on healthy or cancer cell lines. Thus, the synthesized CQD-Au NP system could be considered a biocompatible system. Comparing the SSNP systems with commercial dyes, the SSNPs come with several functionalities due to the commercial dyes. First of all, commercial dyes are not easily water-soluble; they require toxic solvents d No preliminary work is required for SSNP's nano-hybrid particles, whereas cell tracking dyes present several problems, such as their low reproducibility and the need for several optimizations before use [70].

The application of SSNP's nanohybrid particles is quite straightforward. Also, the SSNP's system does not require significant pre-optimizations. Mixing SSNP's nanohybrid particles with fresh culture medium provides sustained stabilization. Cell tracker dyes also need to be applied at the beginning of the cell seeding process. Each time a cell divides, the fluorescent emission from the cell tracker is shared directly across the cell division because the dyes are shared with two daughter cells during cell division [71]. Therefore, SSNP's nano-hybrid particle system is dissolved in the medium, so each divided cell could absorb from the medium, so photofluorescence levels do not change directly day by day. On the other hand,

cell tracker dyes show toxic effects on cells because too long application causes cellular cytotoxicity. Therefore, the application of cell tracker dyes must be optimized in advance [72]. However, the CQD-Au NP system shows no proliferative or cytotoxic effects on healthy or cancer cell lines.

Thus, the synthesized CQD-Au NP system could be considered a biocompatible system. ue to the water. Which could create cellular cytotoxicity. Also, commercial dyes are generally dose-dependently toxic to the cells, whereas SSNPs are not toxic at high doses. Secondly, commercial dyes are easily effected by light itself, with their PL capacity decreasing with time of light accumulation; however, SSNP's system is not affected by light, so it can be used more easily than commercial dyes. Because all of the experiments have been made without considering the environmental light, all of the SSNP's stocks have been kept on the bench without enclosure. Thirdly, commercial dyes require pre-treatments to be applied to the cell. Such live cell imaging dyes require pre-serum-free media treatment, so it takes too much time to apply them to the experiments. However, SSNP's system can be applied into the cell with only adding the media to provide proper staining. [72].

Due to the production process, SSNP's systems are heated to 160°C in the reaction chamber to initiate nucleation and growth. After cooling, they are generally put at room temperature; however, organic commercial dyes require several handling conditions, such as DAPI, which is handled at -20 °C.Also, their thermal stability is generally really low. However, with the heat inoculation or cooling CD-based systems, only PL capacity has been reversibly changed due to the temperature conditions. Increasing the temperature of the CD systems decreases the PL capacity; however, cooling down the same CDs shows the same PL when compared with an untreated CD. [73]. Due to the quantum confinement effect, CD have the unique ability to adjusment the emitted light wavelength with adjusment of their size. So that if the SSNP's fragments can be produced in different sizes, they can be used in different applications or by different molecular trackers [74]. In this research, the main goal is to show that the metal-enhanced AuNP's CD systems, which are made with solid-state reactions, have bioimaging capacity. However, in this research, their optimized working time is not found properly.Main disadvantage of the using SSNP's system is they are not targetted molecules. They can penetrate with any cells. So that they have the limitation of that perspective howver in the literature several solution was applied into the CD's to increase the selectivity of the CD. Such as using aptamer sequences. Aptamer sequences are uniqe

polymerized DNA structures that they are shoing the ability to bind specific cells or specific protein, lipids in the cell. So that combining with the aptamer sequences with CD yang et at has been created MCF-7 cell specific CD system [75].

Doping in chemistry is basically introducing very small amounts of different atoms into one structure. Introducing can be made by adding directly into the structure, or it can be made by bonding ionically or covalently. Adding different atoms to the chemical structure directly affects the physical or chemical properties of the nanostructures. In CDs, single-atom doping and heteroatom doping are two strategies to increase the photoluminescence capacity of the CD. For that reason, several atoms were introduced into the CDs, such as nitrogen, boron, iron, magnesium, and more. Also, introducing different atoms into the system during synthesis can increase the general yield of the system [76]. In this study, the main goal is to increase the photoluminescence capacity with metal enhancement. However, other strategies were not tried. So that introducing different single atoms or heteroatoms in the reaction may increase the overall photoluminescence capacity of the system.

On the other hand, in this study, CD was produced using CA and EDA as a carbon source. But CD can be prepared by using natural products as a carbon source such as ginger. Li et all have been showing that ginger-based produced CD could directly kill cancer cells without needing any different treatment. Also, this CD system can be used for bio-imaging properties too [77]. So the SS methodology could be also used for producing multimodal CD/AuNP

5. CONCLUSION AND FUTURE ASPECTS

In this study, a new approach to synthesize CD/AuNP hybrid material is introduced. The results of the current study indicate that our new approach involving a one-pot solid-state synthesis can produce hybrid materials with enhanced photoluminescent properties. We have seen that the presence of gold enhances the emission properties of the material by locally enhancing the incident excitation due to surface plasmon resonance properties of gold. The hybrid material, denoted as CQD/AuNP, demonstrates also high cytocompatibility with both healthy and cancer cell lines, making it suitable for bioimaging applications. The staining efficiency of the hybrid material is also high, indicating its potential as a staining agent for cell imaging. Moreover, the method for preparing the samples is simple and less time-consuming compared to traditional cell staining methods.

For the future aspect of this study first in in vitro applications. CD /AuNP particles showed that there were no significant differences in the uptake capacity of both healthy and cancer cell lines. To improve the cancer bioimaging properties of the system, selective biomarker molecules should be attached to the system to increase the selectivity of CD /AuNP particles for cancer cells. Beside that uptake mechanism of the CD /AuNP particles should be evaluated for understanding the mechanism. This mechanism could be used for basic step for bio-imaging studies. Also with using peptide or oligonucleotide library generation method CD /AuNP particles can be bind with specific protein ligands to enhancing the bio-imaging quality for specific biomarker for many different illnesses such as cancer. On the other hand, after producing selective CD /AuNP particles, this molecular system should be studied with an in vivo cancer model to understand how the system functions in the tumour microenvironment. Due to the improved permeability and retention effect, all CD /AuNP particles could accumulate in the tumour microenvironment, which could increase the bioimaging capacity of the particles in the in vivo model.Enhanced glycolysis is considered a dominant alteration in tumorigenesis of pancreatic cancer; however, the promotion of metastasis requires enhanced OXPHOS in PDAC [64, 65]. Therefore, the energy crisis-related metabolic switch to glycolysis from OXPHOS by ST treatment might be a promising result for PDAC therapy to decline metastasis progression without affecting normal cells. Migration tests should be performed to reveal the effect of the metabolic switch led by ST on metastasis.

REFERENCES

1. Li HY, Zhao SN, Zang SQ, Li J. Functional metal–organic frameworks as effective sensors of gases and volatile compounds. *Chemical Society Reviews.* 2020;49(17):6364–401.
2. Chang B-J, Manton JD, Sapoznik E, Pohlkamp T, Terrones TS, Welf ES, et al. Real-time multi-angle projection imaging of Biological Dynamics. *Nature Methods*. 2021;18(7):829–34. doi:10.1038/s41592-021-01175-7
3. Huang Z, Qiu L, Zhang T, Tan W. Integrating DNA nanotechnology with aptamers for biological and biomedical applications. *Matter*. 2021;4(2):461–89. doi:10.1016/j.matt.2020.11.002
4. Resch-Genger U, Grabolle M, Cavaliere-Jaricot S, Nitschke R, Nann T. Quantum dots versus organic dyes as fluorescent labels. *Nature Methods*. 2008 Sep;5(9):763-75. doi: 10.1038/nmeth.1248.
5. Kovalenko MV, Protesescu L, Bodnarchuk MI. Properties and potential optoelectronic applications of lead halide perovskite nanocrystals. *Science*. 2017;358(6364):745–50. doi:10.1126/science.aam7093
6. Lei Y, Chen Y, Zhang R, Li Y, Yan Q, Lee S, et al. A fabrication process for flexible single-crystal perovskite devices. *Nature.* 2020;583(7818):790–5. doi:10.1038/s41586-020-2526-z
7. Tu Y, Zhao Z, Lam JWY, Tang BZ. Aggregate science: Much to explore in the meso world. *Matter*. 2021;4(2):338–49. doi:10.1016/j.matt.2020.12.005
8. Long C, Jiang Z, Shangguan J, Qing T, Zhang P, Feng B. Applications of carbon dots in environmental pollution control: A Review. *Chemical Engineering Journal.* 2021;406:126848. doi:10.1016/j.cej.2020.126848
9. Chan M-H, Chen B-G, Ngo LT, Huang W-T, Li C-H, Liu R-S, et al. Natural carbon nanodots: Toxicity assessment and theranostic biological application. *Pharmaceutics.* 2021;13(11):1874. doi:10.3390/pharmaceutics13111874
10. Wang H, Zhang M, Ma Y, Wang B, Huang H, Liu Y, et al. Carbon dots derived from citric acid and glutathione as a highly efficient intracellular reactive oxygen species scavenger for alleviating the lipopolysaccharide-induced inflammation in macrophages. *ACS Applied Materials & Interfaces*. 2020;12(37):41088–95. doi:10.1021/acsami.0c11735

11. Sachdev A, Gopinath P. Green synthesis of multifunctional carbon dots from coriander leaves and their potential application as antioxidants, sensors and bioimaging agents. *The Analyst*. 2015;140(12):4260–9. doi:10.1039/c5an00454c
12. Mansur HS, Mansur AAP, González JC. Synthesis and characterization of cds quantum dots with carboxylic-functionalized poly (vinyl alcohol) for bioconjugation. *Polymer*. 2011;52(4):1045–54. doi:10.1016/j.polymer.2011.01.004
13. Chu K-W, Lee S, Chang C-J, Liu L. Recent progress of carbon dot precursors and photocatalysis applications. *Polymers*. 2019;11(4):689. doi:10.3390/polym11040689
14. Zhao X, Li J, Liu D, Yang M, Wang W, Zhu S, et al. Self-enhanced carbonized polymer dots for selective visualization of lysosomes and real-time apoptosis monitoring. *Science*. 2020;23(4):100982. doi:10.1016/j.isci.2020.100982
15. Han Z, Ni Y, Ren J, Zhang W, Wang Y, Xie Z, et al. Highly efficient and ultra-narrow bandwidth orange emissive carbon dots for microcavity lasers. *Nanoscale*. 2019;11(24):11577–83. doi:10.1039/c9nr03448j
16. Feng X, Ashley J, Zhou T, Sun Y. Fluorometric determination of doxycycline based on the use of carbon quantum dots incorporated into a molecularly imprinted polymer. *Microchimica Acta*. 2018;185(11). doi:10.1007/s00604-018-2999-8
17. Ehrat F, Bhattacharyya S, Schneider J, Löf A, Wyrwich R, Rogach AL, et al. Tracking the source of carbon dot photoluminescence: Aromatic domains versus molecular fluorophores. *Nano Letters*. 2017;17(12):7710–6. doi:10.1021/acs.nanolett.7b03863
18. Huang C-C, Yang Z, Lee K-H, Chang H-T. Synthesis of highly fluorescent gold nanoparticles for sensing mercury(ii). *Angewandte Chemie*. 2007;119(36):6948–52. doi:10.1002/ange.200700803
19. Aminabad NS, Farshbaf M, Akbarzadeh A. Recent advances of gold nanoparticles in biomedical applications: State of the art. *Cell Biochemistry and Biophysics*. 2018;77(2):123–37. doi:10.1007/s12013-018-0863-4
20. Progatzky F, Dallman MJ, Lo Celso C. From seeing to believing: Labelling strategies for in vivo cell-tracking experiments. *Interface Focus*. 2013;3(3):20130001. doi:10.1098/rsfs.2013.0001
21. Wang H, Mararenko A, Cao G, Gai Z, Hong K, Banerjee P, et al. Multifunctional 1D magnetic and fluorescent nanoparticle chains for enhanced MRI, fluorescent cell imaging, and combined photothermal/chemotherapy. *ACS Applied Materials & Interfaces*. 2014;6(17):15309–17. doi:10.1021/am503777k

22. Zhu S, Song Y, Wang J, Wan H, Zhang Y, Ning Y, et al. Photoluminescence mechanism in graphene quantum dots: Quantum confinement effect and surface/edge state. *Nano Today*. 2017;13:10–4. doi:10.1016/j.nantod.2016.12.006
23. Li C, Zhu Y, Zhang X, Yang X, Li C. Metal-enhanced fluorescence of carbon dots adsorbed Ag@SiO2 core-shell nanoparticles. *RSC Advances*. 2012;2(5):1765. doi:10.1039/c2ra01032a
24. Nie H, Li M, Li Q, Liang S, Tan Y, Sheng L, et al. Carbon dots with continuously tunable full-color emission and their application in ratiometric ph sensing. *Chemistry of Materials.* 2014;26(10):3104–12. doi:10.1021/cm5003669
25. Jana J, Aditya T, Ganguly M, Mehetor SK, Pal T. Fluorescence enhancement via varied long-chain thiol stabilized gold nanoparticles: A study of far-field effect. Spectrochimica Acta Part A: *Molecular and Biomolecular Spectroscopy*. 2018;188:551–60. doi:10.1016/j.saa.2017.07.045
26. Li H, Yan X, Kong D, Jin R, Sun C, Du D, et al. Recent advances in Carbon Dots for bioimaging applications. *Nanoscale Horizons*. 2020;5(2):218–34. doi:10.1039/c9nh00476a
27. Sigismund S, Avanzato D, Lanzetti L. Emerging functions of theegfrin cancer. *Molecular Oncology*. 2017;12(1):3–20. doi:10.1002/1878-0261.12155
28. Shapiro GI. Cyclin-dependent kinase pathways as targets for cancer treatment. *Journal of Clinical Oncology*. 2006;24(11):1770–83. doi:10.1200/jco.2005.03.7689
29. Chonghaile TN, Letai A. Mimicking the BH3 domain to kill cancer cells. *Oncogene*. 2008;27(S1). doi:10.1038/onc.2009.52
30. Vinay DS, Ryan EP, Pawelec G, et al. Immune evasion in cancer: Mechanistic basis and therapeutic strategies. *Seminars in Cancer Biology* 2015;35 Suppl:S185-S198. doi:10.1016/j.semcancer.2015.03.004
31. Gupta GP, Massagué J. Cancer metastasis: Building A framework. *Cell*. 2006;127(4):679–95. doi:10.1016/j.cell.2006.11.001
32. Esteves da Silva JCG, Gonçalves HMR. Analytical and bioanalytical applications of carbon dots. *TrAC-Trends Analytical Chemistry* 2011;30(8):1327-36. doi: 10.1016/j.trac.2011.04.009
33. Zhai X, Zhang P, Liu C, Bai T, Li W, Dai L, et al. Highly luminescent carbon nanodots by microwave-assisted pyrolysis. *Chemical Communications*. 2012;48(64):7955.

34. Kang Y, Fang YW, Li Y, Li W, Yin X. Nucleus-staining with biomolecule-mimicking nitrogen-doped carbon dots prepared by a fast neutralization heat strategy *Royal Chemical Society*. 2015 ;51(95):16956–9.
35. Cao L, Wang X, Meziani MJ, Lu F, Wang H, Luo PG, et al. Carbon Dots for Multiphoton Bioimaging. Journal of the *American Chemical Society*. 2007 Sep;129(37):11318–9.
36. Datta R, Ondřej Kozák, Václav Ranc, Markéta Havrdová, Bourlinos AB, Klára Šafářová, et al. Quaternized carbon dot-modified graphene oxide for selective cell labelling – controlled nucleus and cytoplasm imaging *Chemical Communications*. 2014 Aug 19;50(74):10782–2.
37. Ramanan V, Thiyagarajan SK, Raji K, Suresh R, Sekar R, Ramamurthy P. Outright Green Synthesis of Fluorescent Carbon Dots from Eutrophic Algal Blooms for In Vitro Imaging. *ACS Sustainable Chemistry & Engineering*. 2016 Aug 17;4(9):4724–31
38. Licciardello N, Hunoldt S, Bergmann R, Singh G, Mamat C, Faramus A, et al. Biodistribution studies of ultrasmall silicon nanoparticles and carbon dots in experimental rats and tumor mice. *Nanoscale*. 2018;10(21):9880–91.
39. Tao H, Yang K, Ma Z, Wan J, Zhang Y, Kang Z, et al. In Vivo NIR Fluorescence Imaging, Biodistribution, and Toxicology of Photoluminescent Carbon Dots Produced from Carbon Nanotubes and Graphite. *Small.* 2011 Nov 18;8(2):281–90.
40. Buk V, Pemble ME. A highly sensitive glucose biosensor based on a micro disk array electrode design modified with carbon quantum dots and gold nanoparticles. *Electrochimica Acta*. 2019 Mar;298:97–105
41. Lin F, Gui C, Wen W, Bao T, Zhang X. Dopamine assay based on an aggregation-induced reversed inner filter effect of gold nanoparticles on the fluorescence of graphene quantum dots *Talanta*. 2016 Sep 1;158:292–8.
42. Kim J, Park J, Kim H, Singha K, Kim WJ. Transfection and intracellular trafficking properties of carbon dot-gold nanoparticle molecular assembly conjugated with PEI-pDNA. *Biomaterials.* 2013 Sep;34(29):7168–80
43. Liu X, Liu L, Hu X, Zhou S, Ankri R, Fixler D, et al. Multimodal bioimaging based on gold nanorod and carbon dot nanohybrids as a novel tool for atherosclerosis detection. *Nano Research*. 2018 Feb 2;11(3):1262–73.

44. Amendola V, Pilot R, Frasconi M, Maragò OM, Iatì MA. Surface plasmon resonance in gold nanoparticles: a review. Journal of Physics: Condensed *Matter*. 2017 Apr 20;29(20):203002.
45. Bhunia SK, Saha A, Maity AR, Ray SC, Jana NR. Carbon nanoparticle-based fluorescent bioimaging probes. *Scientific reports* . 2013 (cited 2019 Oct 21);3:1473. Available from: https://www.ncbi.nlm.nih.gov/pubmed/23502324
46. Ren G, Zhang Q, Li S, Fu S, Chai F, Wang C, et al. One pot synthesis of highly fluorescent N doped C-dots and used as fluorescent probe detection for Hg2+ and Ag+ in aqueous solution *Sensors and Actuators B: Chemical*,. 2017 May 1;243:244–53.
47. Karg TJ, Golic KG. Photoconversion of DAPI and Hoechst dyes to green and red emitting forms after exposure to UV excitation. *Chromosoma* (Internet). 2018 Jun 1;127(2):235–45. Available from: https://www.ncbi.nlm.nih.gov/pmc/articles/PMC5945337/#:~:text=The%20fluorescent%20dye%204
48. Sk MA, Ananthanarayanan A, Huang L, Lim KH, Chen P. Revealing the tunable photoluminescence properties of graphene quantum dots. *Journal of Materials Chemistry C* (Internet). 2014 Aug 7 (cited 2021 Nov 30);2(34):6954–60. Available from: https://pubs.rsc.org/en/content/articlelanding/2014/tc/c4tc01191k
49. Neikov OD, Yefimov NA. Nanopowders. Handbook of Non-Ferrous Metal Powders. 2019;271–311.
50. Efros AL, Lockwood DJ, Leonid Tsybeskov. Semiconductor Nanocrystals. *Springer Science & Business* Media; 2013.
51. Katan C, Mercier N, Even J. Quantum and Dielectric Confinement Effects in Lower-Dimensional Hybrid Perovskite Semiconductors. *Chemical Reviews*. 2019 Jan 14;119(5):3140–92.
52. Jagtap S, Chopade P, Tadepalli S, Bhalerao A, Gosavi S. A review on the progress of ZnSe as inorganic scintillator. *Opto-Electronics Review*. 2019 Mar;27(1):90–103.
53. Ji X, Wang W, Hedi Mattoussi. Controlling the spectroscopic properties of quantum dots via energy transfer and charge transfer interactions: *Concepts and applications*. 2016 Feb 1;11(1):98–121.
54. Yoshio Kamura, Imura K. Enhanced and Polarized Photoluminescence from Carbon Dot–Metal Nanoparticle *Composites*. 2020 Mar 18;124(13):7370–7.

55. Promofluor Fluorescent Dyes Archives [Internet]. [cited 2023 Aug 11]. Available from: https://promocell.com/product-category/cell-biology/fluorescent-labeling/promofluor-fluorescent-dyes/?filters=10531&sortBy=relevance&type=products
56. Zeliha Cansu Canbek Ozdil, Spalla O, Menguy N, Fabienne Testard. Competitive Seeded Growth: An Original Tool to Investigate Anisotropic Gold Nanoparticle Growth Mechanism *The Journal of Physcial Chemistry*. 2019 Sep 20;123(41):25320–30.
57. Chan GKY, Kleinheinz TL, Peterson D, Moffat JG. A Simple High-Content Cell Cycle Assay Reveals Frequent Discrepancies between Cell Number and ATP and MTS Proliferation Assays. Moreno-Sanchez R, editor. *PLoS ONE*. 2013 May 17;8(5):e63583.
58. Zahra Arab-Bafrani, Daryoush Shahbazi-Gahrouei, Mahdi Abbasian, Mehrafarin Fesharaki. Multiple MTS assay as the alternative method to determine survival fraction of the irradiated HT-29 colon cancer cells *Journal of Medical Signals and Sensors*. 2016 Apr 1;6(2):112–2.
59. Murphy CJ, Gole AM, Stone JW, Sisco PN, Alkilany AM, Goldsmith EC, et al. Gold Nanoparticles in Biology: Beyond Toxicity to Cellular Imaging. *Accounts of Chemical Research*. 2008 Dec 16;41(12):1721–30.
60. Chong Y, Ma Y, Shen H, Tu X, Zhou X, Xu JY, et al. The in vitro and in vivo toxicity of graphene quantum dots. *Biomaterials.* 2014 Jun 1;35(19):5041–8.
61. George SJ, Dwivedi A. MMPs, Cadherins, and Cell Proliferation. Trends in *Cardiovascular Medicine* (Internet). 2004 Apr 1 (cited 2022 Nov 7);14(3):100–5. Available from: https://www.sciencedirect.com/science/article/pii/S1050173803002160
62. Goodwin CJ, Holt SJ, Downes S, Marshall NJ. Microculture tetrazolium assays: a comparison between two new tetrazolium salts, XTT and MTS. *Journal of Immunological Methods*. 1995 Jan;179(1):95–103.
63. Temin HM. The Mechanism of Carcinogenesis by Avian Sarcoma Viruses. I. *Cell Multiplication and Differentiation*2. 1965 Oct 1;
64. Lakshmanan I, Batra S. Protocol for Apoptosis Assay by Flow Cytometry Using Annexin V Staining Method. *BIO-PROTOCOL*. 2013;3(6).
65. Elmore S. Apoptosis: a Review of Programmed Cell Death. *Toxicologic Pathology*. 2007 Jun;35(4):495–516.
66. Welshons WV, Cormier EM, Wolf MS, Williams P, V. Craig Jordan. Estrogen Receptor Distribution in Enucleated Breast Cancer Cell Lines*. 1988 Jun 1;122(6):2379–86.

67. Kang Y, Fang YW, Li Y, Li W, Yin X. Nucleus-staining with biomolecule-mimicking nitrogen-doped carbon dots prepared by a fast neutralization heat strategy *Chemical Communitacion*. 2015 Nov 17;51(95):16956–9.
68. Cao L, Wang X, Meziani MJ, Lu F, Wang H, Luo PG, et al. Carbon Dots for Multiphoton Bioimaging. Journal of the *American Chemical Society*. 2007 Sep;129(37):11318–9.
69. Otto F. Chapter 11 DAPI Staining of Fixed Cells for High-Resolution Flow Cytometry of Nuclear DNA. Flow Cytometry (Internet). 1990 (cited 2019 Nov 18);105–10. Available from: https://www.sciencedirect.com/science/article/pii/S0091679X08605166
70. Zhou W, Kang HC, O'Grady M, Chambers KM, Dubbels B, Melquist P, et al. CellTraceTM Far Red & CellTrackerTM Deep Red. *Journal of Biological Methods*. 2016 Mar 30;3(1):e38.
71. Progatzky F, Dallman MJ, Lo Celso C. From seeing to believing: labelling strategies for in vivo cell-tracking experiments. *Interface Focus* (Internet). 2013 Jun 6 (cited 2021 Dec 12);3(3):20130001. Available from: https://www.ncbi.nlm.nih.gov/pmc/articles/PMC3638420/
72. Wang, B., & Lu, S. (2022). The light of carbon dots: From mechanism to applications. *Matter*, *5*(1), 110-149.
73. Barman, M. K., & Patra, A. (2018). Current status and prospects on chemical structure driven photoluminescence behaviour of carbon dots. *Journal of Photochemistry and Photobiology C: Photochemistry Reviews*, *37*, 1-22.
74. Shi, W., Guo, F., Han, M., Yuan, S., Guan, W., Li, H., ... & Kang, Z. (2017). N, S co-doped carbon dots as a stable bio-imaging probe for detection of intracellular temperature and tetracycline. *Journal of Materials Chemistry B*, *5*(18), 3293-3299.
75. Kong, T., Zhou, R., Zhang, Y., Hao, L., Cai, X., & Zhu, B. (2020). AS1411 aptamer modified carbon dots via polyethylenimine-assisted strategy for efficient targeted cancer cell imaging. *Cell proliferation*, *53*(1), e12713.
76. Miao, S., Liang, K., Zhu, J., Yang, B., Zhao, D., & Kong, B. (2020). Hetero-atom-doped carbon dots: Doping strategies, properties and applications. *Nano Today*, *33*, 100879.
77. Li CL, Ou CM, Huang CC, Wu WC, Chen YP, Lin TE, et al. Carbon dots prepared from ginger exhibiting efficient inhibition of human hepatocellular carcinoma cells. *Journal of Materials Chemistry B*. 2014;2(28):4564.